
Searching Latent Program Spaces

Matthew V Macfarlane*
 University of Amsterdam
 matthew.v.m@live.co.uk

Clément Bonnet*
 Ndeia
 clement.bonnet16@gmail.com

Abstract

General intelligence requires systems that acquire new skills efficiently and generalize beyond their training distributions. Although program synthesis approaches have strong generalization power, they face scaling issues due to large combinatorial spaces that quickly make them impractical and require human-generated DSLs or pre-trained priors to narrow this search space. On the other hand, deep learning methods have had high successes, but they lack structured test-time adaptation and rely on heavy stochastic sampling or expensive gradient updates for fine-tuning. In this work, we propose the Latent Program Network (LPN), a new architecture that builds in test-time search directly into neural models. LPN learns a latent space of implicit programs—neurally mapping inputs to outputs—through which it can search using gradients at test time. LPN combines the adaptability of symbolic approaches and the scalability of neural methods. It searches through a compact latent space at test time and bypasses the need for pre-defined domain-specific languages. On a range of programming-by-examples tasks, LPN either outperforms or matches performance compared to in-context learning and test-time training methods. Tested on the ARC-AGI benchmark, we demonstrate that LPN can both learn a compact program space and search through it at test time to adapt to novel tasks. LPN doubles its performance on out-of-distribution tasks when test-time search is switched on.

1 Introduction

The central goal of artificial intelligence has long been to create generally intelligent systems with human-like cognitive capabilities. While recent years have seen remarkable achievements in narrow AI domains, with systems achieving superhuman performance in games [Campbell et al., 2002, Silver et al., 2017, Vinyals et al., 2019] and specialized tasks [He et al., 2015, Jumper et al., 2021], we face a fundamental challenge: our systems struggle to generalize beyond their training distribution [Yu et al., 2024a] or effectively adapt to novelty [Zhang et al., 2021]. This highlights a critical gap between optimizing for task-specific performance and achieving true general intelligence.

In *On the Measure of Intelligence*, Chollet [2019] argues that traditional benchmarks that measure skills alone are insufficient for developing generally intelligent systems. Such benchmarks can be "gamed" through either unlimited prior knowledge of the task encoded by developers or massive amounts of training data, masking a system's true ability to generalize and adapt. Instead, it is argued we need to measure skill-acquisition efficiency—how effectively a system can learn new tasks with minimal experience—and evaluate generalization capability in a way that controls for both prior knowledge and training data.

By controlling for prior knowledge and experience, the Abstraction and Reasoning Corpus (ARC-AGI) [Chollet, 2019] is a benchmark that measures skill acquisition efficiency rather than pure skills. Its few-shot learning setup requires systems to adapt to novel tasks with very limited data, highlighting

*Equal contribution.

learning efficiency. Importantly, ARC-AGI is designed to evaluate artificial intelligence systems while calibrated to human performance. Therefore, it serves as a useful compass when comparing general intelligence between humans and machines.

Current approaches to solving ARC-AGI and program synthesis benchmarks generally fall into two categories: inductive and transductive methods. (1) Inductive approaches [Parisotto et al., 2016, Devlin et al., 2017b, Butt et al., 2024] infer underlying programs from examples by generating explicit programs using a domain-specific language (DSL). However, handcrafting problem-specific DSLs is inherently unscalable for real-world applications and relies on the unrealistic assumption that a human-generated DSL is always provided. Progress on AI-generated DSLs [Ellis et al., 2021] has also been limited. In this work, we investigate methods that solve problems using only input-output example data. (2) In-context learning—also called transductive—methods [Devlin et al., 2017a, Kolev et al., 2020, Li et al., 2024a] train neural models to condition on a few examples and produce the desired output for a new input, implicitly inferring the program within the model’s activations. These methods benefit from greater scalability by removing the need for a predefined DSL. However, in-context learning struggles with *consistency* [Devlin et al., 2017b], i.e., being able to map the inputs to the outputs of the specification itself. Performing fine-tuning at test time is a powerful way to resolve consistency, but happens to be extremely costly on large models and is also prone to overfitting given limited data [Li et al., 2021]. Additionally, in-context learning in transformers [Vaswani et al., 2017] suffers from the quadratic complexity of self-attention [Hübotter et al., 2024], which hinders scaling specification sizes.

As an attempt to get the best of both inductive and transductive worlds, we introduce the Latent Program Network (LPN), which integrates the benefits of a scalable neural architecture with program induction. By representing implicit programs in a continuous latent space, LPN allows for efficient test-time program search. LPN is more efficient than test-time fine-tuning methods like in Devlin et al. [2017a] because it performs backpropagation only through a fraction of the total parameters. Also, by performing latent program aggregation and recombination in latent space, LPN removes the quadratic cost of attention when scaling specification size.

Our contributions are as follows. (1) We introduce a new architecture named the Latent Program Network (LPN) that builds in test-time adaptation by learning a latent space of programs and searching for the best latent representation given new data. (2) We show that gradient-based latent search during training optimizes the latent space for effective test-time adaptation, yielding significant performance improvements. (3) We demonstrate that LPN generalizes to specification sizes beyond those seen during training, even improving performance, unlike in-context learning, which fails to generalize without parameter fine-tuning at large specification sizes.

2 Related Work

The challenge of navigating vast program spaces has driven diverse approaches to program synthesis. Early researchers focused on deductive methods, using theorem-proving techniques to construct provably correct programs based on formal specifications [Manna and Waldinger, 1980]. However, the difficulty of obtaining formal specifications led to a shift toward inductive approaches [Solomonoff, 1964]. These methods instead infer programs from input-output examples [Shaw et al., 1975, Summers, 1977, Biermann, 1978], making program synthesis more practical for real-world applications.

However, for real-world problems, the exponential search space is a significant challenge for inductive program synthesis methods [Lee et al., 2018]. Three distinct paradigms have emerged to narrow down the search space, all leveraging learning. (1) Researchers have developed differentiable programming languages that integrate symbolic reasoning with continuous optimization [Feser et al., 2016, 2017, Gaunt et al., 2017]. (2) Neural networks have been trained as priors to constrain the search space and enhance the efficiency of program search techniques [Balog et al., 2016, Devlin et al., 2017b]. In this paradigm of leveraging neural priors for search, large language models (LLMs) have been demonstrated to be valuable for navigating complex search spaces, including discrete program synthesis [Wang et al., 2024, Li et al., 2024d, Barke et al., 2024]. CodeIt [Butt et al., 2024] leverages the pre-trained CodeT5 model [Wang et al., 2023] to guide discrete program search. (3) In-context/transductive approaches bypass intermediate program representations entirely by (meta-) training neural networks to directly map input to output examples and a new input

to its corresponding output [Devlin et al., 2017a,b, Kolev et al., 2020]. Neural networks offer a fully differentiable program representation, allowing program induction through gradient descent in parameter space, where network weights encode the program structure [Graves, 2014, Zaremba and Sutskever, 2014, Neelakantan et al., 2015, Kaiser and Sutskever, 2015, Kurach et al., 2015]. While early research focused on learning individual programs, more recent works have broadened the scope to learning multiple programs [Devlin et al., 2017a, Kolev et al., 2020, Li et al., 2024a]. Pre-trained LLMs can also be used to perform transductive reasoning, where they directly generate outputs from specifications included in the prompt—a process known as in-context learning [Gendron et al., 2023, Mitchell et al., 2023, Li et al., 2024a, Brown et al., 2020]. Recent works by Hendel et al. [2023], Yang et al. [2024] demonstrate the emergence of task vectors within LLM activations. LPN advances this approach by explicitly learning and disentangling the program space from other activation information. This separation yields two benefits: enhanced program representations and more efficient program space exploration. While such neural approaches eliminate the need for formal programming languages or DSLs, they sacrifice both interpretability and the ability to perform systematic search during inference. As Devlin et al. [2017b] demonstrated, neural approaches struggle to maintain *consistency* with given specifications and underperform compared to neural-symbolic methods [Parisotto et al., 2016].

Recent work has explored fine-tuning model parameters at test time—test-time training (TTT)—to resolve this inability to be consistent with the specification [Devlin et al., 2017a, Hottung et al., 2021b, Hübotter et al., 2024, Li et al., 2024a, Akyürek et al., 2024]. TTT treats the network parameters as a program, where test-time fine-tuning becomes a search through program space via parameter optimization. Since neural networks are universal function approximators [Hornik et al., 1989], the target program is likely to exist somewhere in this parameter space. Meta-learning approaches such as MAML [Finn et al., 2017], perform gradient updates on few-shot data in the full parameter space. LEO [Rusu et al., 2018] similar to our work explore a version of MAML, introducing a bottleneck, such that the inner loop optimisation is performed in latent space. Their decoder is then a hypernetwork [Ha et al., 2016] which conditions on the latent to generate the raw parameters for inference. LPN removes the need for such a hypernetwork leveraging the in-context learning abilities of transformers to directly perform generation conditioned on the latent variable.

Conditioning neural models on latent spaces has emerged as a powerful approach across diverse domains. Latent space optimization has been applied to molecule generation [Gómez-Bombarelli et al., 2018] and combinatorial optimization challenges, including the traveling salesman problem [Hottung et al., 2021a, Chalumeau et al., 2023]. Recent work has extended latent-based approaches to black-box optimization through energy-based models [Yu et al., 2024b], and symbolic mathematics, where latent optimization helps balance equation complexity with accuracy [Meidani et al., 2023]. In program synthesis, LEAPS [Trivedi et al., 2021] demonstrated how reinforcement learning could search latent program spaces for Karel programs [Pattis, 1994].

LPN can be interpreted through the lens of semi-amortised variational inference (SVI) [Kim et al., 2018, Marino et al., 2018]. SVI operates in two phases: first, it performs amortized variational inference using an encoder trained on the complete dataset. Then, for each data point, it performs additional updates to minimize the amortization gap [Gershman and Goodman, 2014]—the discrepancy between the log-likelihood and the evidence lower bound (ELBO) [Krishnan et al., 2018, Cremer et al., 2018]. The LPN equivalent of these updates for test examples is performing gradient descent in the latent space.

3 Background

Program Synthesis aims to generate deterministic programs in a target language, such that outputs generated from inputs are consistent with the given specification. Typically, the problem space Y consists of programs formulated within a domain-specific language (DSL). Each task is defined by a specification set X , where each specification, $X_m \in X$, is described by a set of input/output (I/O) examples:

$$X_m = \{(x_1^m, y_1^m), \dots, (x_n^m, y_n^m)\} \quad (1)$$

A program $f \in Y$ is considered to solve the task associated with X_m if it satisfies: $\forall j \in [1, n], f(x_j^m) = y_j^m$. This definition requires that the program replicates the output for each input in the specification. We denote F_m to represent the true function that generates the I/O pairs.

Program Synthesis Generalization. We consider the problem of applying a learned program to a new input rather than explaining the specification. Given a set of input-output examples generated by a program F_m (not necessarily constrained to a DSL), along with an additional input x_{n+1}^m ,

$$P_m = \{(x_1^m, y_1^m), \dots, (x_n^m, y_n^m), x_{n+1}^m\}. \quad (2)$$

The objective is to generalize from the provided examples and predict the corresponding output for x_{n+1}^m . This can be done via induction or transduction [Li et al., 2024a]. If we do not limit the Kolmogorov complexity of programs [Kolmogorov, 1965, Solomonoff, 1964], we can find an explanation for any given specification, whether or not it corresponds to the true program that underlies the specification. Evaluating generalization performance not only tests the ability to explain a specification but also whether it can successfully infer the underlying program in its generality and apply it to a new input. This problem bears a resemblance to few-shot learning, with the difference of having only one task. The ARC-AGI benchmark [Chollet, 2019] falls under this program synthesis formulation. Each of its tasks is composed of input-output pairs represented as 2D grid of shape up to 30x30, whose cells can take any of 10 colors.

4 Latent Program Network (LPN)

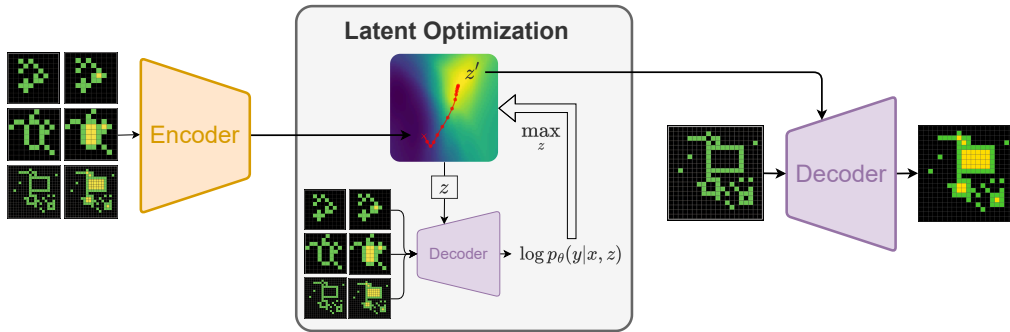


Figure 1: Inference of the Latent Program Network (LPN) model. (Left): the encoder maps I/O pairs to a latent space of encoded programs. (Middle): the latent program is refined during an optimization process to best explain the given I/O pairs (figure detailed in the appendix at Figure 18). (Right): the decoder executes the latent program to generate the desired output for a newly given input.

Prior work tackling programming by example with a neural approach has focused on directly training models to maximize the likelihood of decoding the correct output given a specification (in context) [Kolev et al., 2020]. However, we diverge from such transduction-based methods, as they cannot inherently adapt at test time or ensure specification consistency. Instead, we explicitly factorize inference into three core components visualized in Figure 1. First, we introduce a bottleneck that encourages the network to learn an explicit representation of programs via a compact latent space. Secondly, we introduce a method for searching this latent space to explain the given data effectively. Lastly, conditioned on the latent program and a new input, we predict the output. Despite this added structure, the Latent Program Network (LPN) remains fully differentiable end-to-end. This structure provides several key benefits. Firstly, explicitly learning program representations acts as a good neural network prior for generalization. Secondly, we can use this program encoding to verify that our initial guess for a latent program explains the given data. If not, the program latent can be refined at test-time to best explain the given data. Lastly, LPN removes issues faced by transductive approaches that overfit to specification sizes (number of input-output pairs) seen during training.

4.1 Latent Program Inference

LPN is composed of three core architectural components to perform inference. A neural encoder, a neural decoder, and a latent space optimization. In this section, we discuss each component and then outline how to train the full system in later sections.

Encoder. The probabilistic encoder is trained to approximate the Bayesian posterior over program latents. Specifically, it maps an input-output pair (x, y) to a distribution in the latent space $q_\phi(z|x, y)$,

representing possible programs that could explain the given input-output mapping. Using a variational approach is important because, for any given input-output pair, there exists a broad range of possible programs that map the input to the output, even when restricting to, e.g., programs of low Kolmogorov complexity [Solomonoff, 1964, Kolmogorov, 1965]. We discuss LPN as semi-amortised variational inference in Appendix D. Intuitively, the encoder is trained to learn an abstract representation of programs in a continuous latent space by implicitly encoding input-output pair examples. In practice, we use a multivariate normal distribution whose mean μ and diagonal covariance Σ parameters are inferred by the encoder. To take advantage of hardware parallelization, the encoder can process all the I/O pairs in a given specification in parallel. By encoding each pair independently and aggregating using the mean LPN is permutation invariant to the specification order, as opposed to a naive sequence model that would concatenate I/O pairs.

Decoder. The probabilistic decoder is responsible for mapping a latent program and an input to its expected corresponding output, directly predicting the output pixel-by-pixel instead of via a DSL. It models the distribution of possible outputs y given an input x and a latent z . Note that even if the underlying I/O mappings are deterministic, we still use a probabilistic decoding framework $p_\theta(y|x, z)$ to be compatible with maximum likelihood learning. Figure 18 shows the decoder generating different outputs by keeping the input fixed but varying the latent program, which in this figure represents a specific grid pattern to reproduce. In a real task, the aim of this encoder-decoder system is to learn a compressed representation of the space of possible programs we care about (e.g., in the case of ARC-AGI, this would correspond to programs that use the Core Knowledge priors [Chollet, 2019]).

Latent Optimization. The encoder is trained to approximate the posterior over programs and may not encode the right abstraction given an I/O pair. Especially if the task is very novel, the encoder may fail at producing the right latent program, which, fed to the decoder, would generate the wrong output. Therefore, we include a middle stage of latent optimization where, starting from the encoder’s prediction z , we search for a better latent program z' , one that would better explain the observed data according to the decoder p_θ . The search process is generally denoted $z' = f(p_\theta, z, x, y)$ and can be implemented in several ways (c.f. section 4.2). Analogous to system 1 / system 2 thinking [Kahneman, 2011], we can think of the encoder generating an intuitive first guess as to what the observed program may be (system 1), and the latent optimization process executing a search for hypotheses that would better explain the observations (system 2). See Appendix C for test-time inference pseudo-code.

$$\begin{array}{lll} \text{Encoder} & \text{Latent Optimization} & \text{Decoder} \\ z \sim q_\phi(z|x, y) & z' = f(p_\theta, z, x, y) & \hat{y} \sim p_\theta(y|x, z') \end{array} \quad (3)$$

4.2 Search Methods for Latent Optimization

Given n input-output pairs $\{(x_i, y_i)\}_{i=1\dots n}$, the search process $z' = f(p_\theta, z, x, y)$ attempts to find a z' that satisfies:

$$z' \in \arg \max_z \sum_{i=1}^n \log p_\theta(y_i|x_i, z) \quad (4)$$

This means we search for the latent that would most likely make the decoder generate the right outputs given the corresponding inputs. By finding a latent that can explain all the input-output pairs, the latent solution to the optimization problem is more likely to generalize to a new input-output pair. We describe here two instantiations of the search process, namely a *sampling* and a *gradient ascent* algorithm, both acting in the latent space of programs. We leave for future work the exploration of other search methods like evolutionary strategies [Hansen and Ostermeier, 2001, Chalumeau et al., 2023] that could better trade-off exploration and exploitation of the latent space.

Sampling. A naive version of the latent search process is to sample a batch of latents from either the prior distribution $p(z)$ or around the approximate Bayesian posterior $q_\phi(z|x_i, y_i)$ and select the latent that gives the highest log likelihood of decoding the given input-output pairs. Specifically, for all $k \in [1, K]$, $z_k \sim p(z)$, and we select $z' \in \arg \max_{z_k} \sum_{i=1}^n \log p_\theta(y_i|x_i, z_k)$. *Sampling* asymptotically converges to the true maximum-likelihood latent (equation 4) and can prove useful when the function to optimize (here, the decoder log-likelihood) is not differentiable. However, the efficiency of sampling-based search decreases exponentially with the dimension of the latent space, which makes it impractical for most applications.

Gradient Ascent. Since the decoder is a differentiable neural network, its log-likelihood $\log p_\theta(y|x, z)$ is also differentiable with respect to z and one can use first-order methods like gradient-ascent to efficiently search through the latent space for a solution to the latent optimization problem (equation 4, see Figure 18 for a visualization of a 2D latent space trained on grid patterns). This visualization highlights that only a small portion of the latent space can explain all the input-output pairs, corresponding to high decoding likelihood. Notably, poor initialization can lead the search to converge to different local minima, highlighting the importance of amortized inference from the encoder. We initialize z'_0 as the mean of all the pair latents sampled from the encoder, and refine it iteratively as follows:

$$\forall k \in [1, K], \quad z'_k = z'_{k-1} + \alpha \cdot \nabla_z \sum_{i=1}^n \log p_\theta(y_i | x_i, z) \Big|_{z=z'_{k-1}} \quad (5)$$

The series $(z'_k)_{k \in [1, K]}$ should exhibit increasing decoding likelihood if the step size α is small enough. In practice, we generate the output with the best latent found during the gradient ascent algorithm, which may not always be the one that is obtained after taking the last gradient step (z'_K).

4.3 Training

To train the LPN system end-to-end, we assume we have a dataset of tasks, where a task is defined as n input-output pairs (x_i, y_i) generated by the same program. To simulate the test conditions of predicting a new input from a given specification, we design the training procedure to reconstruct each of the outputs y_i from their inputs x_i and all the $n - 1$ other pairs $(x_j, y_j)_{j \neq i}$. We emphasize that we do not use the specific pair (x_i, y_i) to reconstruct y_i , which would lead to the encoder directly compressing the output y_i as a shortcut without learning program-related abstractions.

When reconstructing output y_i , we first sample latents z_j from the encoder $q_\phi(z|x_j, y_j)$ for all $j \neq i$. We then aggregate them by computing their mean $\frac{1}{n-1} \sum_{j \neq i} z_j$, then we perform latent optimization using e.g., gradient ascent to obtain z'_i . Finally, we compute the negative log-likelihood of the right output y_i using its corresponding input x_i and the refined latent z'_i . In practice, we compute the cross-entropy loss of the decoder logits $p_\theta(\hat{y}_i|x_i, z'_i)$ and the labels y_i , which is derived from maximizing the likelihood of a categorical distribution. The full training pipeline is detailed in Appendix C. Specifically, we compute the reconstruction loss \mathcal{L}_{rec} and the KL loss \mathcal{L}_{KL} between the approximate posterior and the prior:

$$\mathcal{L}_{\text{rec}}(\phi, \theta) = \sum_{i=1}^n -\log p_\theta(y_i | x_i, z'_i) \quad \mathcal{L}_{\text{KL}}(\phi) = \sum_{i=1}^n D_{\text{KL}}(q_\phi(z|x_i, y_i) \parallel \mathcal{N}(0, I)) \quad (6)$$

The dependence of the reconstruction loss $\mathcal{L}_{\text{rec}}(\phi, \theta)$ in ϕ arises from using the reparameterization trick [Kingma, 2013] when sampling each latent z_j . Indeed, we first sample a normal random vector $\epsilon_j \sim \mathcal{N}(0, I)$, then we infer the mean μ_j and diagonal covariance Σ_j using the encoder and recompose the latent $z_j = \mu_j + \epsilon_j \cdot \Sigma_j$. Then, z'_i is used by the decoder to reconstruct the output. Note that we can decide whether to let the decoder gradient flow through the latent update. Indeed, it is more computationally efficient to stop the gradient through the update, by changing line 9 of algorithm 2 with $z'_i = z'_i + \alpha \cdot \overline{g'_i}$, where $g'_i = \nabla_z \sum_{j \neq i} \log p_\theta(y_j | x_j, z) \Big|_{z=z'_i}$, with $\overline{g'_i}$ notating a stop-gradient on g'_i .

We denote β as the weighting factor that balances the reconstruction and KL terms [Burgess et al., 2018], which gives the combined training objective: $\mathcal{L}_{\text{total}}(\phi, \theta) = \mathcal{L}_{\text{rec}}(\phi, \theta) + \beta \mathcal{L}_{\text{KL}}(\phi)$. This training procedure offers some freedom in the latent optimization, i.e., how to compute z'_i from z_i . Training with gradient ascent latent optimization (as detailed in Algorithm 2) incurs a compute overhead due to the cost of the latent gradient computation through the decoder. Although we may use a high compute budget at test-time, we propose to use a small number of gradient ascent steps during training, ranging from 0 to 5 steps.

Training	Inference					
	Grad 0	Grad 1	Grad 5	Grad 20	Grad 100	Sample 250
Grad 0	3.2 (2.7)	3.6 (3.0)	18.8 (14.4)	52.5 (25.0)	67.5 (20.0)	3.2 (2.7)
Grad 1	8.6 (4.4)	44.6 (10.9)	85.4 (7.6)	98.4 (1.4)	99.5 (0.5)	10.2 (5.3)
Grad 1 **	0.6 (0.1)	13.7 (3.0)	60.2 (7.5)	88.9 (6.0)	94.1 (3.8)	0.7 (0.2)
Grad 5	0.0 (0.0)	0.4 (0.3)	31.9 (11.2)	88.5 (11.9)	98.1 (2.1)	0.5 (0.4)
Sample 5	6.1 (4.4)	8.2 (6.5)	27.7 (21.6)	56.3 (27.5)	72.2 (21.2)	6.1 (4.4)

Table 1: Ablation of LPN training and inference methods on the *Pattern* task. Rows/columns represent different training/inference methods, differing only in the latent optimization. "Grad [N]" stands for N gradient ascent steps, "Sample [N]" for N samples from the encoder distribution without leveraging any gradients, and "Grad 1 **" means that the decoder parameter gradient flows through the latent optimization update. Training was performed for 20k steps with 3 seeds, aggregating performance as mean (and standard deviation in brackets) over the 3 runs. Bold values indicate the best training method for each inference regime. See expanded table in Appendix B.1

5 Experiments

5.1 Setup

We consider the ARC-AGI 2024 challenge [Chollet et al., 2024] as the testing domain for our method. This program synthesis benchmark encompasses diverse tasks designed to test adaptation and out-of-distribution generalization, rather than memorization. We implement both the LPN encoder and decoder as small transformers [Vaswani et al., 2017], see Appendix G for full architecture details. We fully open-source the codebase used to run all experiments in the paper in the supplementary material. We introduce the simpler *Pattern* task to investigate LPN’s dynamics before large-scale ARC-AGI training, see Appendix A. It generates 10x10 black input grids with a blue pixel indicating where a 4x4 program-specific pattern should be pasted. This task is sufficient to demonstrate weaknesses in deep learning models that do not leverage test-time computation (see Section 5.4).

Baselines. We compare LPN to an in-context learning method Kolev et al. [2020], Li et al. [2024a], which encodes each of the input-output pairs and then concatenates these embeddings to condition output prediction, notably never producing any intermediate program embeddings. We discuss the motivation for this design in Appendix H. Then, we also compare to test-time fine-tuning [Devlin et al., 2017a, Akyürek et al., 2024], which, given a test-time specification, performs parameter-based gradient updates on the in-context model. See Appendix H for details on baseline implementations and Appendix E for hyperparameters.

5.2 Pattern Task

We compare a variety of LPN training and inference methods in Table 1, to better understand the dynamics of LPN. We aim to first answer whether LPN can self-improve at test-time by searching its latent space, and then how the training inference strategy affects performance. For each training method, we train a small 1M parameter model for 20k steps with a batch size of 128 and evaluate it with different inference modes. We find that inference using no test-time adaptation performs poorly across all instances of LPN (and in-context baselines, see Appendix B.2). This shows that amortizing inference is difficult for models of this size and training time.

All variations of LPN training show strong scaling in performance as the number of gradient steps at test time is scaled. This demonstrates that LPN is capable of test-time adaptation to improve pre-trained amortization performance. We visualise the decoded outputs at many points in the latent space of LPN on a simple pattern task in Appendix B.4 showing structure in the latent program representations, and Appendix B.4 shows the likelihood of the specification is smooth across the space, enabling gradient based test time search.

When comparing different LPN training inference strategies, 1 gradient ascent step of latent optimization shows higher returns than training with mean pooling, with the difference particularly pronounced when scaling the inference budget. With 100 steps of gradient ascent at inference time, LPN training with grad 0 gets an accuracy of 67.5%, whereas training with one gradient step (Grad

1) reaches 99.5%. This demonstrates the benefits of training the latent space with the awareness that gradient ascent will be performed at test-time, an important inductive bias for the LPN architecture. We also observe that gradient ascent vastly outperforms sampling-based search, validating that a search without any gradient signal is highly inefficient. Lastly we perform training with and without the stop gradient on the gradient update itself. We found that using the stop gradient actually leads to higher test time performance while also being more computationally efficient.

5.3 Starting test-time search from the encoder

In addition, we ablate the impact of initializing latent optimization with the encoder versus using the prior, in order to assess the benefits of amortizing inference. In Figure 2, we specifically compare no latent search (blue), to doing latent optimization in two ways: sampling from the prior $z \sim p(z)$ (orange), and sampling from the encoder $z \sim q_\phi(z|x, y)$ (green). Initializing latent search with the encoder is critical for performance across all training methods. This validates the intuition that LPN can perform fast system 1-like reasoning using the encoder and then narrow down the search space during latent optimization, simulating system 2 reasoning.

5.4 Adapting Out-Of-Distribution

A significant challenge to deep learning methods is generalizing to out-of-distribution (OOD) tasks. We study the OOD behavior of LPN, in-context learning, and parameter fine-tuning on the *Pattern* task in Table 2. In-context learning has no test time adaptation performance as it has no inherent mechanism to scale compute beyond a single forward pass. We include full experiments on a range of varying OOD settings in Appendix B.2. When trained with 1 step of gradient ascent, LPN recovers high accuracy (88%) using 100 steps of gradient ascent at inference time. TTT and in-context learning are incapable of recovering the right OOD pattern at inference time. We perform a similar experiment in Appendix B.7 on a synthetic integer sequence task with less spatial structure, with the same conclusions.

5.5 Scaling Specification

For any learning method that can handle varying amounts of data, an important question is how the method scales to handling more data than it was trained on. In Figure 3 we evaluate in-context learning, TTT, and LPN with and without gradient search in the OOD setting of the *pattern* task, with varying specification sizes. LPN smoothly generalizes to different specification sizes, with only a small drop in performance with less data, and keeps improving with more data. In-context learning overfits to the specification size it is trained on, and TTT only performs well once given a sufficiently large specification and high inference compute. We ablate this in Appendix B.5, repeating the experiment for varying training specification sizes.

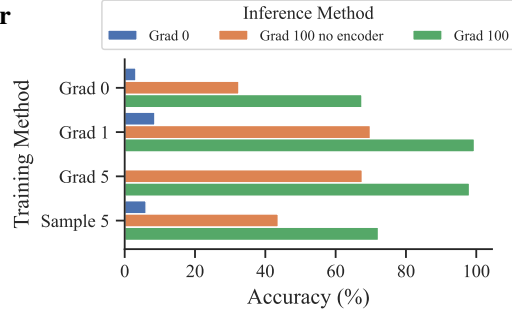


Figure 2: Ablation on the role of the encoder and latent optimization. Latents are initialized from the mean of the encoder latents (except for orange). *Grad N* stands for doing latent optimization with N gradient steps. Both the encoder initialization and the latent optimization matter for LPN.

Training	Inference		
	Grad 0	Grad 10	Grad 100
In-Context	0.0 (0.0)	-	-
TTT	0.0 (0.0)	1.8 (0.7)	0.3 (0.1)
LPN Grad 0	0.3 (0.5)	18.8 (14.5)	41.1 (29.6)
LPN Grad 1	0.0 (0.0)	59.9 (11.6)	88.0 (5.3)
LPN Grad 2	0.0 (0.0)	38.5 (13.0)	81.8 (10.9)

Table 2: Out-of-distribution (OOD) performance on the *Pattern* task. Performance is averaged over 3 training runs with different seeds, with standard deviation in parentheses.

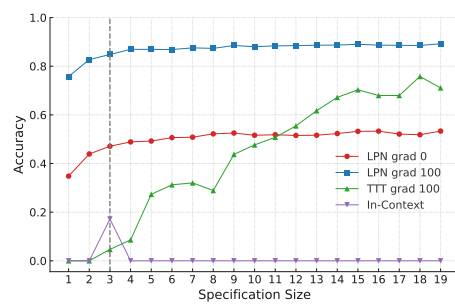


Figure 3: Scaling specification sizes on the OOD pattern task.

FLOPs	In-Distribution				Out-of-Distribution			
	LPN	TTT	CodeIt	Mirchandani	LPN	TTT	CodeIt	Mirchandani
2E+11	68.75	45.75	-	-	7.75	5.85	-	-
2E+12	75.95	51.75	-	-	10.25	7.35	-	-
2E+13	80.00	58.50	-	-	15.25	13.50	-	-
2E+14	76.25	58.75	-	-	15.50	16.00	-	-
2E+15	78.50	57.00	-	-	15.50	15.25	-	-
» 2E+15	-	-	-	14.00	-	-	14.75	6.75

Table 3: Results on ARC-AGI for varying values of FLOPs. In-Distribution refers to puzzles in the ARC train set not trained on but are in-distribution relative to re-ARC. Out-of-distribution refers to puzzles from the eval set. LPN and TTT stand for Latent Program Network (**ours**), and Test-Time Training. CodeIt and Mirchandani are baselines from prior work.

5.6 ARC-AGI 2024

Setup We train on the `re-arc` dataset [Hodel, 2024], designed to be in distribution relative to the ARC training set (which we don’t train on) Li et al. [2024b]. The evaluation set is significantly OOD, representing a challenging generalization experiment. We train a 178M-parameter LPN with a 256-dim latent space for 100k steps for 2 days on a TPU v4-32, see Appendix E. Leveraging insights from pattern task experiments, we use gradient ascent in LPN during training. To remain efficient, we train LPN in Grad 0 mode for 95k steps and then fine-tune in Grad 1 for a further 5k steps, which we find gives a marginal boost in performance at lower levels of test time compute Appendix B.8.

Results Table 3 shows top-2 accuracy on ARC-AGI (standard to ensure resolvability of all problems). Even after significant amortization of inference, we observe large performance gains from scaling gradient search at test time. LPN significantly outperforms TTT in-distribution. We also see strong evidence that the LPN has learned a structured latent space for representing programs, demonstrated by a t-SNE plot of the embeddings of different programs in the training set, see Appendix F. Out of distribution, LPN doubles its performance by using latent space search at test-time (scaling FLOPs from 2e11 to 2e15). Using from 2E+11 to 2E+13 FLOPs, LPN outperforms TTT, until we scale test-time compute to much higher levels, where TTT achieves higher performance. This finding is likely due to the lack of diversity in programs seen by LPN during training, relative to experiments on other datasets, limiting the ability to have a smooth expressive latent space. Relative to the pattern task, TTT is less susceptible to overfitting on ARC-AGI, possibly due to the use of larger model sizes. Both methods outperform two ARC specific LLM approaches that leverage far larger pre-trained models, including CodeT5 [Butt et al., 2024] (220M parameters) and text-davinci [Mirchandani et al., 2023] (175B parameters). This work represents an improvement over such methods due to significantly lower inference and training cost, and greater generalization from limited training distribution. The current highest performing model on ARC-AGI is o3-preview(low) (LLM) which achieves 75.7% at a cost of \$200 per task. Both the training and inference costs are far beyond this work, there is an opportunity for future work to investigate scaling up this work to such a scale.

6 Conclusion

We introduced Latent Program Network (LPN), a novel approach to inductive program synthesis leveraging continuous latent spaces for efficient test-time adaptation. LPN integrates adaptation directly into its architecture, refining latent representations through gradient-based search, which we identify as an efficient adaptation method. We show that LPN generalizes beyond the training distribution, relying on test-time adaptation rather than expanded synthetic datasets.

Limitations and Future Work. A limitation of this work is the limited diversity of programs on which LPN is trained. While augmentations are used during training, the distribution of programs remains narrow and restricts the potential for learning an expressive complex latent space. We limit gradient-based search to standard optimizers. Future work could explore alternative optimization methods, such as evolution strategies, and explore discrete program representations to enhance compositional generalization.

7 Acknowledgments and Disclosure of Funding

We thank Google’s TPU Research Cloud (TRC) for supporting this research. We are also grateful to Nathan Grinsztajn, Natasha Butt, Levi Lelis, and Jessica Hu for their feedback on the early versions of the paper. Matthew Macfarlane is supported by the LIFT-project 019.011, which is partly financed by the Dutch Research Council (NWO). We also thank reviewers for their detailed feedback which we have integrated into the final version of the paper.

References

Ekin Akyürek, Mehul Damani, Linlu Qiu, Han Guo, Yoon Kim, and Jacob Andreas. The surprising effectiveness of test-time training for abstract reasoning. *arXiv preprint arXiv:2411.07279*, 2024.

Alexei Baevski and Michael Auli. Adaptive input representations for neural language modeling. *arXiv preprint arXiv:1809.10853*, 2018.

Matej Balog, Alexander L Gaunt, Marc Brockschmidt, Sebastian Nowozin, and Daniel Tarlow. Deepcoder: Learning to write programs. *arXiv preprint arXiv:1611.01989*, 2016.

Shraddha Barke, Emmanuel Anaya Gonzalez, Saketh Ram Kasibatla, Taylor Berg-Kirkpatrick, and Nadia Polikarpova. Hysynth: Context-free llm approximation for guiding program synthesis. *arXiv preprint arXiv:2405.15880*, 2024. URL <https://arxiv.org/abs/2405.15880>.

Alan W Biermann. The inference of regular lisp programs from examples. *IEEE transactions on Systems, Man, and Cybernetics*, 8(8):585–600, 1978.

Tom B. Brown, Benjamin Mann, Nick Ryder, Melanie Subbiah, Jared Kaplan, Prafulla Dhariwal, Arvind Neelakantan, Pranav Shyam, Girish Sastry, Amanda Askell, Sandhini Agarwal, Ariel Herbert-Voss, Gretchen Krueger, Tom Henighan, Rewon Child, Aditya Ramesh, Daniel M. Ziegler, Jeffrey Wu, Clemens Winter, Christopher Hesse, Mark Chen, Eric Sigler, Mateusz Litwin, Scott Gray, Benjamin Chess, Jack Clark, Christopher Berner, Sam McCandlish, Alec Radford, Ilya Sutskever, and Dario Amodei. Language models are few-shot learners. *Advances in Neural Information Processing Systems*, 33:1877–1901, 2020.

Christopher P Burgess, Irina Higgins, Arka Pal, Loic Matthey, Nick Watters, Guillaume Desjardins, and Alexander Lerchner. Understanding disentangling in β -vae. *arXiv preprint arXiv:1804.03599*, 2018.

Natasha Butt, Blazej Manczak, Auke Wiggers, Corrado Rainone, David W Zhang, Michaël Defferrard, and Taco Cohen. Codeit: Self-improving language models with prioritized hindsight replay. *arXiv preprint arXiv:2402.04858*, 2024.

Murray Campbell, A Joseph Hoane Jr, and Feng-hsiung Hsu. Deep blue. *Artificial intelligence*, 134(1-2):57–83, 2002.

Felix Chalumeau, Shikha Surana, Clément Bonnet, Nathan Grinsztajn, Arnu Pretorius, Alexandre Laterre, and Tom Barrett. Combinatorial optimization with policy adaptation using latent space search. *Advances in Neural Information Processing Systems*, 36:7947–7959, 2023.

Francois Chollet, Mike Knoop, Bryan Landers, Greg Kamradt, Hansueli Jud, Walter Reade, and Addison Howard. Arc prize 2024. <https://kaggle.com/competitions/arc-prize-2024>, 2024. Kaggle.

François Chollet. On the measure of intelligence, 2019. URL <https://arxiv.org/abs/1911.01547>.

Chris Cremer, Xuechen Li, and David Duvenaud. Inference suboptimality in variational autoencoders. In *International conference on machine learning*, pages 1078–1086. PMLR, 2018.

Jacob Devlin, Rudy R Bunel, Rishabh Singh, Matthew Hausknecht, and Pushmeet Kohli. Neural program meta-induction. *Advances in Neural Information Processing Systems*, 30, 2017a.

Jacob Devlin, Jonathan Uesato, Surya Bhupatiraju, Rishabh Singh, Abdel-rahman Mohamed, and Pushmeet Kohli. Robustfill: Neural program learning under noisy i/o. In *International conference on machine learning*, pages 990–998. PMLR, 2017b.

Kevin Ellis, Catherine Wong, Maxwell Nye, Mathias Sablé-Meyer, Lucas Morales, Luke Hewitt, Luc Cary, Armando Solar-Lezama, and Joshua B Tenenbaum. Dreamcoder: Bootstrapping inductive program synthesis with wake-sleep library learning. In *Proceedings of the 42nd ACM SIGPLAN international conference on programming language design and implementation*, pages 835–850, 2021.

John K Feser, Marc Brockschmidt, Alexander L Gaunt, and Daniel Tarlow. Differentiable functional program interpreters. *arXiv preprint arXiv:1611.01988*, 2016.

John K Feser, Marc Brockschmidt, Alexander L Gaunt, and Daniel Tarlow. Neural functional programming. 2017.

Chelsea Finn, Pieter Abbeel, and Sergey Levine. Model-agnostic meta-learning for fast adaptation of deep networks. In *International conference on machine learning*, pages 1126–1135. PMLR, 2017.

Alexander L Gaunt, Marc Brockschmidt, Nate Kushman, and Daniel Tarlow. Differentiable programs with neural libraries. In *International Conference on Machine Learning*, pages 1213–1222. PMLR, 2017.

Gaël Gendron, Qiming Bao, Michael Witbrock, and Gillian Dobbie. Large language models are not strong abstract reasoners. *arXiv preprint arXiv:2305.19555*, 2023.

Samuel Gershman and Noah Goodman. Amortized inference in probabilistic reasoning. In *Proceedings of the annual meeting of the cognitive science society*, volume 36, 2014.

Rafael Gómez-Bombarelli, Jennifer N Wei, David Duvenaud, José Miguel Hernández-Lobato, Benjamín Sánchez-Lengeling, Dennis Sheberla, Jorge Aguilera-Iparraguirre, Timothy D Hirzel, Ryan P Adams, and Alán Aspuru-Guzik. Automatic chemical design using a data-driven continuous representation of molecules. *ACS central science*, 4(2):268–276, 2018.

Alex Graves. Neural turing machines. *arXiv preprint arXiv:1410.5401*, 2014.

David Ha, Andrew Dai, and Quoc V Le. Hypernetworks. *arXiv preprint arXiv:1609.09106*, 2016.

Nikolaus Hansen and Andreas Ostermeier. Completely derandomized self-adaptation in evolution strategies. *Evolutionary Computation*, 9(2):159–195, 2001. doi: 10.1162/106365601750190398.

Kaiming He, Xiangyu Zhang, Shaoqing Ren, and Jian Sun. Delving deep into rectifiers: Surpassing human-level performance on imagenet classification. In *Proceedings of the IEEE international conference on computer vision*, pages 1026–1034, 2015.

Roee Hendel, Mor Geva, and Amir Globerson. In-context learning creates task vectors. *arXiv preprint arXiv:2310.15916*, Oct 2023. URL <https://arxiv.org/abs/2310.15916>.

Michael Hodel. Addressing the abstraction and reasoning corpus via procedural example generation, 2024. URL <https://arxiv.org/abs/2404.07353>.

Kurt Hornik, Maxwell Stinchcombe, and Halbert White. Multilayer feedforward networks are universal approximators. *Neural networks*, 2(5):359–366, 1989.

André Hottung, Bhanu Bhandari, and Kevin Tierney. Learning a latent search space for routing problems using variational autoencoders. In *International Conference on Learning Representations*, 2021a.

André Hottung, Yeong-Dae Kwon, and Kevin Tierney. Efficient active search for combinatorial optimization problems. *arXiv preprint arXiv:2106.05126*, 2021b.

Jonas Hübotter, Sascha Bongni, Ido Hakimi, and Andreas Krause. Efficiently learning at test-time: Active fine-tuning of llms. *arXiv preprint arXiv:2410.08020*, 2024.

John Jumper, Richard Evans, Alexander Pritzel, Tim Green, Michael Figurnov, Olaf Ronneberger, Kathryn Tunyasuvunakool, Russ Bates, Augustin Žídek, Anna Potapenko, et al. Highly accurate protein structure prediction with alphafold. *nature*, 596(7873):583–589, 2021.

Daniel Kahneman. *Thinking, fast and slow*. 1st ed. New York : Farrar, Straus and Giroux, [2011] ©2011, 2011. URL <https://search.library.wisc.edu/catalog/9910114919702121>. Includes bibliographical references (pages 447-448) and index.

Łukasz Kaiser and Ilya Sutskever. Neural gpus learn algorithms. *arXiv preprint arXiv:1511.08228*, 2015.

Yoon Kim, Sam Wiseman, Andrew Miller, David Sontag, and Alexander Rush. Semi-amortized variational autoencoders. In *International Conference on Machine Learning*, pages 2678–2687. PMLR, 2018.

Diederik P Kingma. Auto-encoding variational bayes. *arXiv preprint arXiv:1312.6114*, 2013.

Victor Kolev, Bogdan Georgiev, and Svetlin Penkov. Neural abstract reasoner. *arXiv preprint arXiv:2011.09860*, 2020.

Andrei Nikolaevich Kolmogorov. Three approaches to the definition of the concept “quantity of information”. *Problemy peredachi informatsii*, 1(1):3–11, 1965.

Rahul Krishnan, Dawen Liang, and Matthew Hoffman. On the challenges of learning with inference networks on sparse, high-dimensional data. In *International conference on artificial intelligence and statistics*, pages 143–151. PMLR, 2018.

Karol Kurach, Marcin Andrychowicz, and Ilya Sutskever. Neural random-access machines. *arXiv preprint arXiv:1511.06392*, 2015.

Woosuk Lee, Kihong Heo, Rajeev Alur, and Mayur Naik. Accelerating search-based program synthesis using learned probabilistic models. *ACM SIGPLAN Notices*, 53(4):436–449, 2018.

Shaohua Li, Xiuchao Sui, Jie Fu, Huazhu Fu, Xiangde Luo, Yangqin Feng, Xinxing Xu, Yong Liu, Daniel SW Ting, and Rick Siow Mong Goh. Few-shot domain adaptation with polymorphic transformers. In *Medical Image Computing and Computer Assisted Intervention–MICCAI 2021: 24th International Conference, Strasbourg, France, September 27–October 1, 2021, Proceedings, Part II 24*, pages 330–340. Springer, 2021.

Wen-Ding Li, Keya Hu, Carter Larsen, Yuqing Wu, Simon Alford, Caleb Woo, Spencer M Dunn, Hao Tang, Michelangelo Naim, Dat Nguyen, et al. Combining induction and transduction for abstract reasoning. *arXiv preprint arXiv:2411.02272*, 2024a.

Wenhai Li, Yudong Xu, Scott Sanner, and Elias Boutros Khalil. Tackling the abstraction and reasoning corpus with vision transformers: the importance of 2d representation, positions, and objects. *arXiv preprint arXiv:2410.06405*, 2024b.

Wenhai Li, Yudong Xu, Scott Sanner, and Elias Boutros Khalil. Tackling the abstraction and reasoning corpus with vision transformers: the importance of 2d representation, positions, and objects, 2024c. URL <https://arxiv.org/abs/2410.06405>.

Yixuan Li, Julian Parsert, and Elizabeth Polgreen. Guiding enumerative program synthesis with large language models. In *International Conference on Computer Aided Verification*, pages 280–301. Springer, 2024d.

Zohar Manna and Richard Waldinger. A deductive approach to program synthesis. *ACM Transactions on Programming Languages and Systems (TOPLAS)*, 2(1):90–121, 1980.

Joe Marino, Yisong Yue, and Stephan Mandt. Iterative amortized inference. In *International Conference on Machine Learning*, pages 3403–3412. PMLR, 2018.

Kazem Meidani, Parshin Shojaee, Chandan K Reddy, and Amir Barati Farimani. Snip: Bridging mathematical symbolic and numeric realms with unified pre-training. *arXiv preprint arXiv:2310.02227*, 2023.

Suvir Mirchandani, Fei Xia, Pete Florence, Brian Ichter, Danny Driess, Montserrat Gonzalez Arenas, Kanishka Rao, Dorsa Sadigh, and Andy Zeng. Large language models as general pattern machines. *arXiv preprint arXiv:2307.04721*, 2023.

Melanie Mitchell, Alessandro B Palmarini, and Arseny Moskvichev. Comparing humans, gpt-4, and gpt-4v on abstraction and reasoning tasks. *arXiv preprint arXiv:2311.09247*, 2023.

Arvind Neelakantan, Quoc V Le, and Ilya Sutskever. Neural programmer: Inducing latent programs with gradient descent. *arXiv preprint arXiv:1511.04834*, 2015.

Emilio Parisotto, Abdel-rahman Mohamed, Rishabh Singh, Lihong Li, Dengyong Zhou, and Pushmeet Kohli. Neuro-symbolic program synthesis. *arXiv preprint arXiv:1611.01855*, 2016.

Richard E Pattis. *Karel the robot: a gentle introduction to the art of programming*. John Wiley & Sons, 1994.

Andrei A Rusu, Dushyant Rao, Jakub Sygnowski, Oriol Vinyals, Razvan Pascanu, Simon Osindero, and Raia Hadsell. Meta-learning with latent embedding optimization. *arXiv preprint arXiv:1807.05960*, 2018.

David E Shaw, William R Swartout, and C Cordell Green. Inferring lisp programs from examples. In *IJCAI*, volume 75, pages 260–267, 1975.

David Silver, Thomas Hubert, Julian Schrittwieser, Ioannis Antonoglou, Matthew Lai, Arthur Guez, Marc Lanctot, Laurent Sifre, Dharshan Kumaran, Thore Graepel, et al. Mastering chess and shogi by self-play with a general reinforcement learning algorithm. *arXiv preprint arXiv:1712.01815*, 2017.

Ray J Solomonoff. A formal theory of inductive inference. part i. *Information and control*, 7(1):1–22, 1964.

Jianlin Su, Murtadha Ahmed, Yu Lu, Shengfeng Pan, Wen Bo, and Yunfeng Liu. Roformer: Enhanced transformer with rotary position embedding. *Neurocomputing*, 568:127063, 2024.

Phillip D Summers. A methodology for lisp program construction from examples. *Journal of the ACM (JACM)*, 24(1):161–175, 1977.

Dweep Trivedi, Jesse Zhang, Shao-Hua Sun, and Joseph J Lim. Learning to synthesize programs as interpretable and generalizable policies. *Advances in neural information processing systems*, 34: 25146–25163, 2021.

Ashish Vaswani, Noam Shazeer, Niki Parmar, Jakob Uszkoreit, Llion Jones, Aidan N. Gomez, Łukasz Kaiser, and Illia Polosukhin. Attention is all you need. *Advances in Neural Information Processing Systems*, 2017.

Oriol Vinyals, Igor Babuschkin, Wojciech M Czarnecki, Michaël Mathieu, Andrew Dudzik, Junyoung Chung, David H Choi, Richard Powell, Timo Ewalds, Petko Georgiev, et al. Grandmaster level in starcraft ii using multi-agent reinforcement learning. *nature*, 575(7782):350–354, 2019.

Evan Wang, Federico Cassano, Catherine Wu, Yunfeng Bai, Will Song, Vaskar Nath, Ziwen Han, Sean Hendryx, Summer Yue, and Hugh Zhang. Planning in natural language improves llm search for code generation. *arXiv preprint arXiv:2409.03733*, 2024. URL <https://arxiv.org/abs/2409.03733>.

Yue Wang, Hung Le, Akhilesh Deepak Gotmare, Nghi DQ Bui, Junnan Li, and Steven CH Hoi. Codet5+: Open code large language models for code understanding and generation. *arXiv preprint arXiv:2305.07922*, 2023.

Ruixin Xiong, Yunchang Yang, Di He, Kai Zheng, Shuxin Zheng, Chen Xing, Huishuai Zhang, Yanyan Lan, Liwei Wang, and Tie-Yan Liu. On layer normalization in the transformer architecture, 2020. URL <https://arxiv.org/abs/2002.04745>.

Liu Yang, Ziqian Lin, Kangwook Lee, Dimitris Papailiopoulos, and Robert D. Nowak. Task vectors in in-context learning: Emergence, formation, and benefits. *arXiv preprint arXiv:2501.09240*, Jan 2024. URL <https://arxiv.org/abs/2501.09240>.

Han Yu, Jiashuo Liu, Xingxuan Zhang, Jiayun Wu, and Peng Cui. A survey on evaluation of out-of-distribution generalization. *arXiv preprint arXiv:2403.01874*, 2024a.

Peiyu Yu, Dinghuai Zhang, Hengzhi He, Xiaojian Ma, Ruiyao Miao, Yifan Lu, Yasi Zhang, Deqian Kong, Ruiqi Gao, Jianwen Xie, et al. Latent energy-based odyssey: Black-box optimization via expanded exploration in the energy-based latent space. *arXiv preprint arXiv:2405.16730*, 2024b.

Wojciech Zaremba and Ilya Sutskever. Learning to execute. *arXiv preprint arXiv:1410.4615*, 2014.

Chiyuan Zhang, Samy Bengio, Moritz Hardt, Benjamin Recht, and Oriol Vinyals. Understanding deep learning (still) requires rethinking generalization. *Communications of the ACM*, 64(3):107–115, 2021.

A Datasets

A.1 Pattern Task

The ARC-AGI challenge contains many diverse programs leveraging different knowledge priors. Injecting these priors into LPN by training the model to master ARC-like tasks requires significant compute resources when training from scratch, without an LLM-based initialization. Therefore, to investigate the training dynamics and properties of LPN before such a large-scale training, we develop a simpler task called *Pattern* task (see figure 4) within the same domain, but using a narrow distribution of pattern-like programs. This specific task always generates fully-black 10×10 inputs with a single blue pixel at a random location that defines where the output pastes a 4×4 pattern sampled from a uniform distribution. The pattern is program-specific, meaning it is the same across different pairs but varies from specification to specification. This task demonstrates how deep learning methods without test-time computation may still make errors on such tasks. We then extend this task to study an out-of-distribution setting in section 5.4.

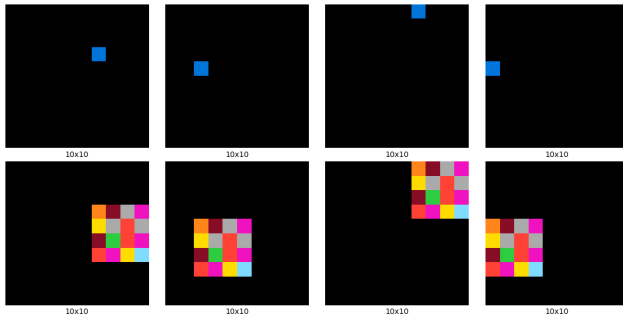


Figure 4: Example of input (top row) and output (bottom row) pairs of a specification sampled from the *Pattern* task. Each sample is a batch of 4 pairs that share the same pattern.

A.2 ARC-AGI

We evaluate LPN on the ARC-AGI benchmark by training it on the `re-arc` dataset [Hodel, 2024], a dataset designed to be in distribution relative to the ARC training set, previously used for training large language models and ARC specific transformers to solve ARC-AGI Li et al. [2024b], Akyürek et al. [2024]. Most previous works however expand beyond this dataset, usually synthetically adding additional programs [Butt et al., 2024], or crafted datasets. We restrict training to tasks from only this dataset with the goal of assessing generalization instead of closing a performance gap with more data. This also ensures LPN solely learns from core knowledge priors without data leakage from the evaluation set. The evaluation set is known to be significantly out of distribution and therefore represents a challenging generalization experiment. We train a 178M-parameter LPN with a 256-dim latent space for 100k steps (batch size 256) for 2 days on a TPU v4-32, see Appendix E for further details, in terms of data, this amounts to 51M I/O pairs. Leveraging insights from smaller scale experiments we make use of gradient in LPN during training. We train LPN in Grad 0 mode for 95k steps and then fine tune in Grad 1 for a further 5k steps. We outline our hyperparameter procedure for both LPN and TTT for ARC-AGI in Appendix E.

B Expanded Experiments

B.1 LPN Training Extended

We provide an expanded version of Table 1 with additional ablations for both the training and inference axes.

Training	Inference					
	Grad 0	Grad 1	Grad 5	Grad 20	Grad 100	Sample 250
Grad 0	3.2 (2.7)	3.6 (3.0)	18.8 (14.4)	52.5 (25.0)	67.5 (20.0)	3.2 (2.7)
Grad 1	8.6 (4.4)	44.6 (10.9)	85.4 (7.6)	98.4 (1.4)	99.5 (0.5)	10.2 (5.3)
Grad 1 **	0.6 (0.1)	13.7 (3.0)	60.2 (7.5)	88.9 (6.0)	94.1 (3.8)	0.7 (0.2)
Grad 5	0.0 (0.0)	0.4 (0.3)	31.9 (11.2)	88.5 (11.9)	98.1 (2.1)	0.5 (0.4)
Grad 5 **	0.0 (0.0)	0.0 (0.0)	9.9 (2.9)	87.1 (6.0)	95.1 (3.3)	0.0 (0.0)
Sample 5	6.1 (4.4)	8.2 (6.5)	27.7 (21.6)	56.3 (27.5)	72.2 (21.2)	6.1 (4.4)
Sample 25	10.8 (8.0)	13.3 (10.1)	39.9 (21.4)	72.3 (18.5)	87.9 (9.2)	10.8 (8.0)

Table 4: Ablation study of LPN training and inference methods on the *Pattern* task. Rows represent training methods: LPN Grad [N] for N gradient steps, LPN Grad [N] ** with gradient flow through latent optimization (analogous to meta-learning), and Sample [N] for N random samples. Columns represent inference methods: Grad [N] for N gradient ascent steps and Sample [N] for random search with N samples. Training was performed for 20k steps with 3 seeds, with performance reported as mean (standard deviation) over 3 runs. Bold values indicate the best performance per inference method.

B.2 Adapting Out-Of-Distribution

We provide expanded results for the out-of-distribution (OOD) experiments outlined in Section 5.4. We include results for varying levels of OOD starting with in-distribution, weak OOD, and strong OOD.

Training	Inference		
	Grad 0	Grad 10	Grad 100
In-Context	15.3 (0.6)	-	-
Test Time Training	15.3 (0.6)	17.0 (1.7)	0.78 (0.69)
LPN Grad 0	30.2 (15.7)	72.8 (29.5)	82.2 (21.3)
LPN Grad 1	26.6 (7.4)	98.0 (0.6)	99.2 (0.6)
LPN Grad 2	14.4 (3.5)	97.2 (1.6)	98.9 (1.2)
LPN Grad 3	1.0 (0.7)	85.7 (6.3)	98.3 (1.9)
LPN Grad 1 **	10.6 (6.4)	93.8 (5.1)	97.4 (1.9)

In-distribution

Training	Inference		
	Grad 0	Grad 10	Grad 100
In-Context	2.1 (0.9)	-	-
Test Time Training	2.1 (0.9)	2.1 (1.1)	0.00 (0.00)
LPN Grad 0	7.6 (5.6)	51.3 (35.7)	62.8 (38.3)
LPN Grad 1	7.4 (4.4)	93.1 (4.3)	97.7 (2.2)
LPN Grad 2	3.0 (2.6)	86.1 (6.0)	95.9 (2.1)
LPN Grad 3	0.0 (0.0)	55.0 (7.8)	93.9 (3.8)
LPN Grad 1 **	1.3 (1.0)	81.7 (13.3)	91.5 (5.5)

Weakly out-of-distribution

Training	Inference		
	Grad 0	Grad 10	Grad 100
In-Context	0.0 (0.0)	-	-
Test Time Training	0.0 (0.0)	1.8 (0.7)	0.3 (0.1)
LPN Grad 0	0.3 (0.5)	18.8 (14.5)	41.1 (29.6)
LPN Grad 1	0.0 (0.0)	59.9 (11.6)	88.0 (5.3)
LPN Grad 2	0.0 (0.0)	38.5 (13.0)	81.8 (10.9)
LPN Grad 3	0.0 (0.0)	11.3 (9.3)	72.0 (14.0)
LPN Grad 1 **	0.0 (0.0)	40.9 (19.8)	71.1 (14.3)

Strongly out-of-distribution

Table 5: Study of the out-of-distribution (OOD) performance on the *Pattern* task. Models are trained on patterns that have a density of 50% (half black, half colored), then evaluated on the same distribution, on a density of 75% (weakly OOD) and 100% (strongly OOD). Performance is averaged over 3 training runs with different seeds, with standard deviation in parentheses.

B.3 Validating the Decoder

Training deep networks from scratch to solve ARC-like tasks has been challenging [Li et al., 2024c]. If it is the case that neural networks struggle even to learn to execute single programs this represents a significant bottleneck to training models from scratch on a broad distribution of programs. Therefore, before training LPN end-to-end, we conclusively show that our decoder architecture does not suffer from such a bottleneck, and can learn individual programs.

We show 5 of the 400 total tasks from the ARC-AGI training set, and for each of these tasks, we train a small LPN architecture of 800k parameters (except for the last task which required a bigger model with 8.7M parameters) on the corresponding task generator from `re-arc` [Hodel, 2024]. Specifically, we select the first five tasks from the `arc-agi_training_challenges` json file (007bbfb7, 00d62c1b, 017c7c7b, 025d127b, 045e512c) shown in figure Figure 5.

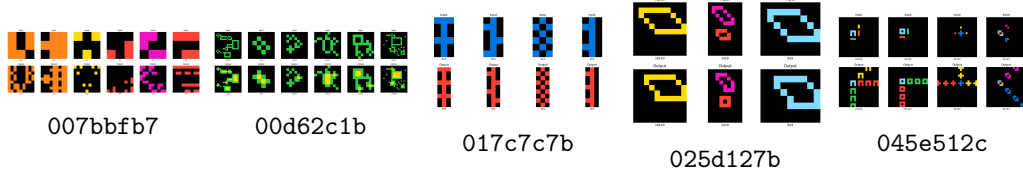


Figure 5: Overfit training on the first 5 ARC-AGI training tasks. The captions correspond to task IDs. For each task, the top row contains the input grids, and the bottom row the output grids. Each task consists of observing all pairs but the first and inferring the output of the leftmost pair given its input. Each curve corresponds to a separate training run.

We evaluate both the distribution of `re-arc` generated tasks on which it is trained and on the true task from the ARC-AGI training set in figure Figure 6. We show that for each task, the small LPN decoder-only model successfully learns individual programs and manages to solve the corresponding ARC-AGI task. Therefore, our model outperforms previously reported results in Li et al. [2024c], and concludes that our architecture does not suffer from a decoder bottleneck. Note that the encoder is not helpful in this experiment since the task is always the same. Our later results on ARC-AGI Section 5.6 take this a step further and show that we can learn a single transformer architecture capable of executing over 270 programs in the ARC training dataset.

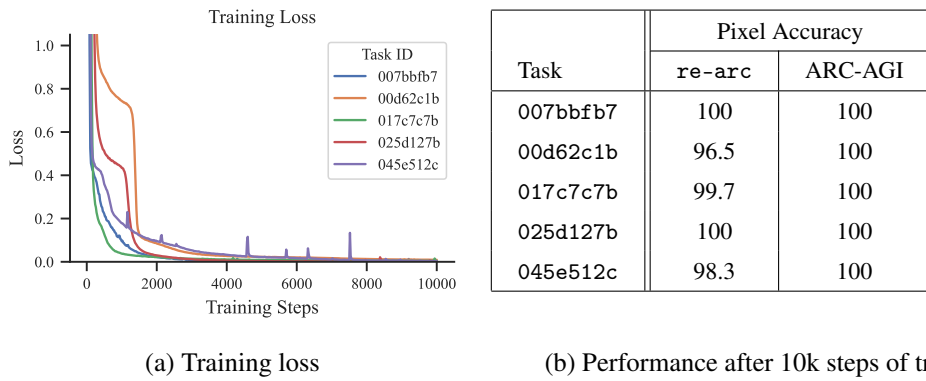


Figure 6: Training loss and performance of LPN training on 5 of the `re-arc` distributions. For each task, only samples from the `re-arc` generators are used for training. The corresponding ARC-AGI tasks are never seen during training.

B.4 Analyzing the Latent Space

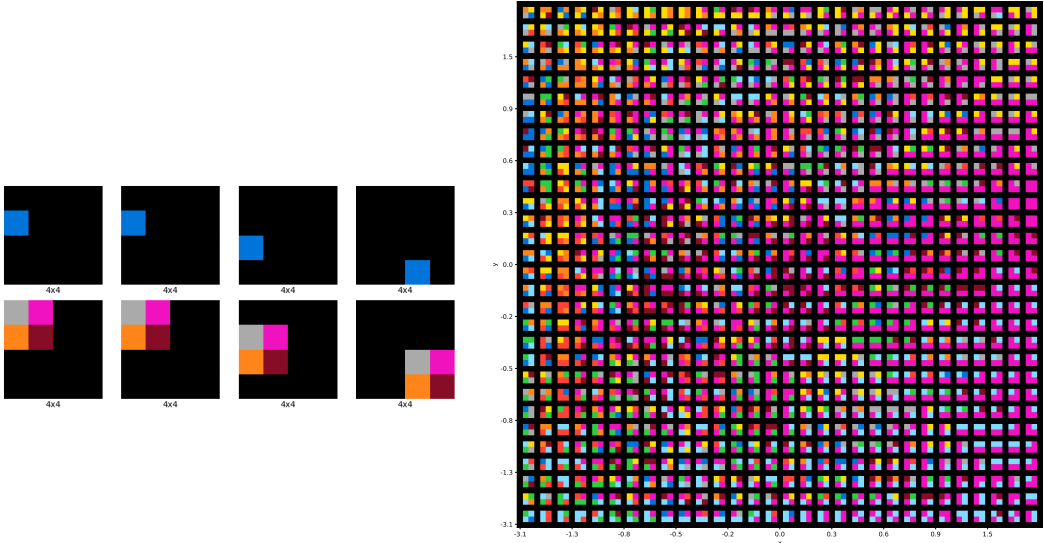
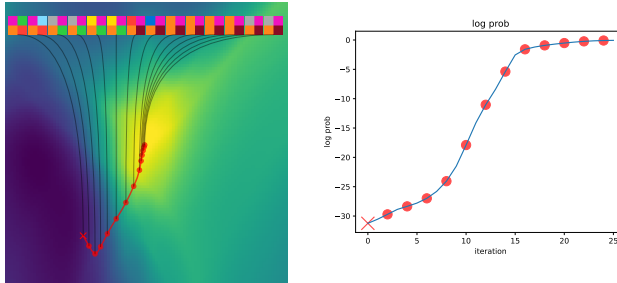


Figure 7: (Left) A 2D pattern task with inputs containing marker points where patterns should be placed, with patterns varying for each program. (Right) The latent traversal visualizes the effect of traversing the latent space, on the predicted pattern by the decoder at marker points.

To validate that the encoder is learning programs in its latent space, we design an even simpler task with small 4x4 grids that have 2x2 patterns. We train a small LPN model until convergence with a latent space of dimension 2 to easily visualize it in figure Figure 7. Due to the simplicity of the task we train the model with *mean* training, i.e. no latent optimization. Because we are using a 2D Gaussian prior for the latent space, we can convert \mathbb{R}^2 to the unit square using the normal cumulative distribution function (CDF), and then plot on the unit square at coordinates (x, y) the decoder’s output when conditioned by the latent $\text{CDF}(z) = (x, y)$, or equivalently, $z = (\text{PPF}(x), \text{PPF}(y))$ using the percent-point function (PPF). These results demonstrate the diversity and smoothness of the latent space, showing structure in terms of color patterns, which motivates performing gradient ascent latent optimization in more complex tasks. This shows that the latent space can encode a wide range of diversity in its latent space which is especially important for adapting to unseen patterns.



The figures on the left show a random initialization in the latent space and a corresponding latent trajectory following the gradient ascent algorithm. The log-likelihood for each latent is shown during optimization. The decoded pattern is traced until convergence in the latent space, giving insights into how LPN performs latent optimization at test time to find the optimal latent program.

B.5 Scaling Specification Size

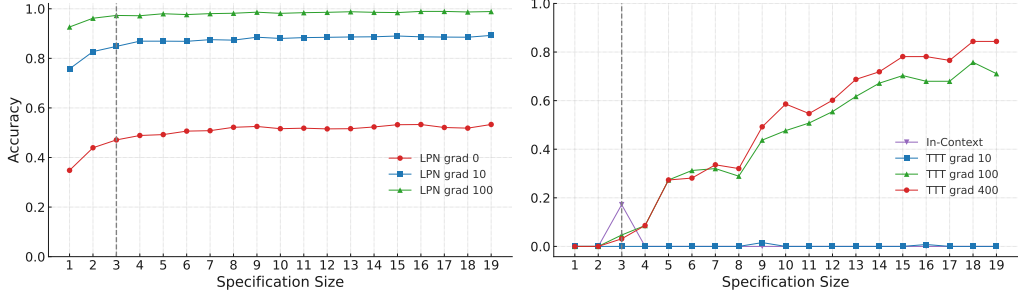


Figure 8: Accuracy of Latent Program Network (LPN) and Test-Time Training (TTT) models as we scale specification size. Higher specification sizes improve accuracy across different training methods. The dashed vertical line at specification size 3 indicates the fixed size used during training.

To analyze the effect of scaling specification size, we conduct an ablation using models trained on the pattern task for a single seed. We compare both in-context learning and LPN. We then evaluate different inference strategies on the in-distribution dataset and analyze their performance as the test specification size increases.

Our results indicate that LPN generalizes effectively across varying specification sizes. This robustness is primarily due to the use of mean pooling, which prevents overfitting to specific context lengths and enables the model to gracefully handle both slightly larger and significantly larger specification sizes. Furthermore, mean pooling encourages representations of the same program to remain structurally similar, improving generalization.

In contrast, in-context learning exhibits strong overfitting to the training specification size, with a noticeable drop in performance as the specification size deviates from the training distribution. However, we observe that fine-tuning-based inference can scale effectively with increasing specification sizes, provided that a sufficient amount of data is available. The effectiveness of fine-tuning is highly dependent on the choice of hyperparameters, requiring substantial amounts of data to maintain strong performance as the specification size grows.

B.5.1 Performance Across Training Sizes

To further explore the impact of training specification size on model performance, we present results for training sizes 1, 7, and 11, evaluated across test sizes 1, 3, 7, 11, 15, and 19 on the pattern task. The following tables report accuracy for LPN with and without gradient ascent, In-Context Learning, and Test-Time Training (TTT). Notably, In-context learning consistently overfits to specific test sizes that align closely with the training size. In contrast, LPN, particularly with 100 gradient ascent steps, demonstrates robust generalization, maintaining high accuracy across all test sizes and training sizes. TTT shows improved performance as test sizes increase, approaching LPN’s accuracy at larger specification sizes when also trained on large specification sizes.

Method	Test Size					
	1	3	7	11	15	19
LPN grad 0	38.9	44.1	47.5	44.7	48.8	45.9
LPN grad 100	89.8	92.1	94.1	94.1	95.3	96.3
In-Context	2.1	0.0	0.0	0.0	0.0	0.0
TTT grad 100	7.8	19.9	50.9	72.4	81.8	90.4

Table 6: Performance (top-2 accuracy, percentage) for training size 1 on the pattern task.

Method	Test Size					
	1	3	7	11	15	19
LPN grad 0	14.6	27.7	32.8	33.4	33.2	35.1
LPN grad 100	87.7	89.3	92.7	91.0	92.6	93.6
In-Context	0.0	0.0	78.3	0.0	0.0	0.0
TTT grad 100	11.3	34.7	77.9	90.6	94.7	93.2

Table 7: Performance (top-2 accuracy, percentage) for training size 7 on the pattern task.

Method	Test Size					
	1	3	7	11	15	19
LPN grad 0	11.1	26.6	40.8	43.2	50.0	48.8
LPN grad 100	91.4	97.1	97.5	96.9	98.0	97.9
In-Context	0.0	0.0	0.1	94.1	0.1	0.0
TTT grad 100	0.1	16.2	56.1	78.3	93.7	92.2

Table 8: Performance (top-2 accuracy, percentage) for training size 11 on the pattern task.

B.6 Measuring Floating Point Operations

To evaluate the computational efficiency of different methods, we measure the number of floating-point operations (FLOPs) required for performing inference on a single task. The reported FLOP measurements correspond to the cost of generating an entire 30×30 grid given 3 input-output pairs (specification size).

While gradient-based approaches do not require an additional computational budget in terms of trial attempts, their inference mechanisms involve performing gradient updates, either in parameter space or latent space, which adds a computational overhead. A key distinction between TTT and LPN is their computational cost: LPN updates only the latent space by backpropagating through the decoder, whereas TTT requires backpropagation through all model parameters. This makes TTT significantly more expensive and less efficient for real-time applications.

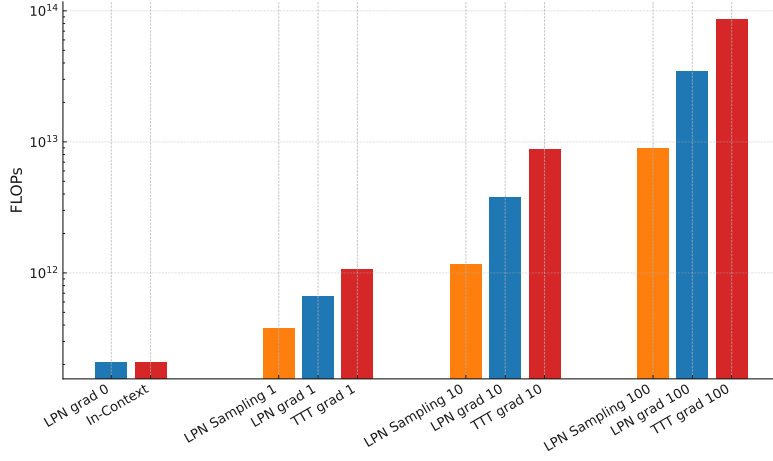


Figure 9: Floating-point operations (FLOPs) required for test-time inference across different methods.

The LPN Sampling results can be understood as ablation of LPN without gradient-based search, but only sampling multiple latents from the encoder computing the decoder likelihood for each, avoiding the computational cost of backpropagating through the decoder. However, this efficiency gain comes at a significant cost in performance, as shown in the pattern task results Table 1.

B.7 Sequence Ablation

B.7.1 Dataset

To investigate the generalizability of our results beyond environments with significant spatial structure, we perform an ablation on a synthetic sequence task and replicate the analysis previously conducted on the pattern dataset. This synthetic dataset features a vast program space, with over 100 million unique programs, each defined by composing 3 to 5 parameterized rules that transform sequences of numbers (ranging from 0 to 4). Programs are composed of 3 to 5 rules with specific integer-based parameters (e.g., thresholds or operation values). These rules are then applied in their chosen order: for each rule, we process the sequence from left to right, transforming each position according to the rule’s condition and operation, producing an intermediate sequence that serves as input to the next rule. This sequential, rule-by-rule application, with each rule scanning left to right, enables complex transformations and vast numbers of programs with meaningfully different outputs. The core rules are defined as follows:

- If a number is greater than its right neighbor by a threshold k , decrease it by a value m , modulo 5.
- If a number has identical neighbors on both sides, multiply its value by a factor n and clip the result to 4.
- If a number is greater than its left neighbor by a threshold k , add a value m , modulo 5.
- If a number is less than its right neighbor by a threshold k , subtract a value m , modulo 5.
- Replace the number with a function of its neighbors (e.g., sum, average, maximum, or minimum), modulo 5.

These parameterized rules may interact at the same position across their sequential applications, creating cascading effects that result in complex transformations. While a single input-output pair may not uniquely identify the underlying program, multiple pairs typically provide sufficient information to determine it. The table below presents accuracy metrics for models evaluated on this task.

B.7.2 Results

Our experiments demonstrate that Test-Time Training (TTT) exhibits overfitting, as evidenced by their performance degradation when gradient fine tuning is performed. In contrast, LPN maintains robust performance without overfitting. Furthermore, incorporating a single gradient step during training enhances LPN performance marginally at higher inference gradients.

Training	Inference (Avg \pm Std)		
	Grad 0	Grad 10	Grad 100
In-Context	0.78 (0.01)	-	-
Test-Time Training	0.78 (0.01)	0.73 (0.01)	0.12 (0.01)
LPN Grad 0	0.76 (0.02)	0.83 (0.01)	0.81 (0.01)
LPN Grad 1	0.71 (0.00)	0.86 (0.01)	0.82 (0.02)
LPN Grad 2	0.63 (0.01)	0.85 (0.00)	0.80 (0.01)
LPN Grad 3	0.49 (0.04)	0.85 (0.00)	0.82 (0.02)
LPN Grad 1 **	0.68 (0.01)	0.85 (0.00)	0.81 (0.01)

Table 9: Study of model performance across different inference gradients for methods: In-Context, Test-Time Training with learning rate of 1e-4, LPN Grad 0, LPN Grad 1, LPN Grad 2, LPN Grad 3 (all with learning rates of 1e-1), LPN Grad 1 **. Performance is averaged over 3 training runs, with standard deviation in parentheses.

B.8 LPN fine tuning

We also ablate LPN training by training in full Grad 0 mode for 100k steps. We show the results compared to fine tuning for 5k steps in Grad 1 mode.

FLOPs	LPN Grad 1 Tune	LPN Grad 0 Tune
2E+11	7.75	8.25
2E+12	10.25	10.25
2E+13	15.25	13.60
2E+14	15.50	15.10
2E+15	15.50	15.10

Table 10: Performance of LPN with and without gradient tuning on ARC-AGI for 10k steps

We find a marginal performance gain at higher computational budgets from fine-tuning with one gradient step, so we adopt this approach in the main method. However, we note a slight performance drop in Grad 0 inference, which is expected as the network begins to optimize with gradient adaptation.

B.9 ARC-AGI Solution Analysis

In this section we investigate whether there are differences between the types of tasks in ARC-AGI evaluation dataset that LPN solves vs Test-Time Training. We run both methods at the budget of $2E+14$ and analyze the problems solved. We first analyze the overlap between problems solved between the two methods. We see that there is a spread of the different problems being solved by the different architectures, a roughly even split between problems only solved by TTT, problems solved only by LPN and problems solved by both.

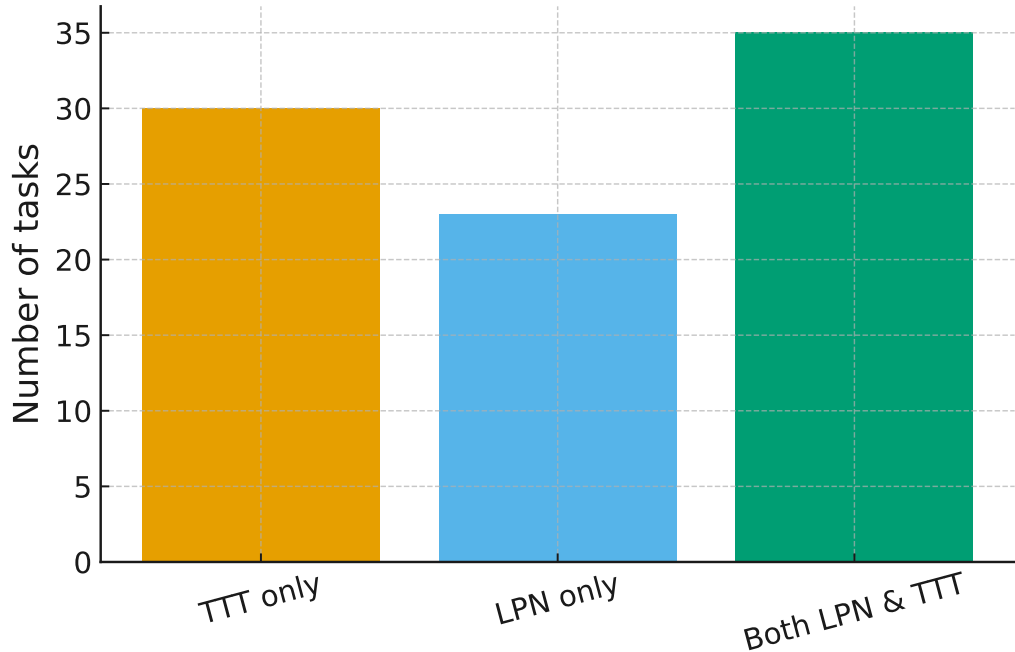


Figure 10: Bar Chart showing Problems Uniquely solved by LPN and TTT and tasks solved when at least one solves the problem

If we measure the accuracy when either LPN or TTT solves an ARC puzzle. We achieve a combined score of 22%. We also show 3 examples of problems solved only by LPN and 3 examples only solved by Test-Time Training to understand the differences between the problems each method solved.

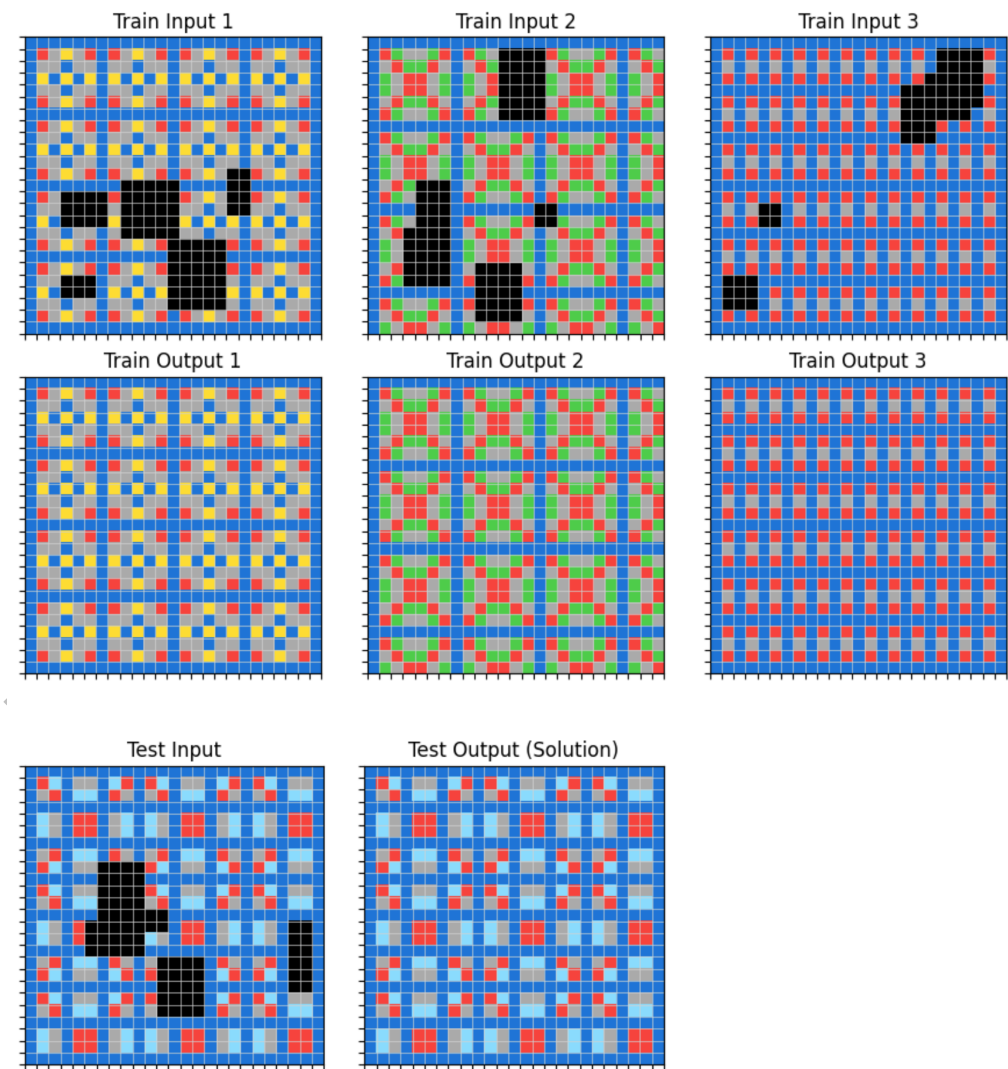


Figure 11: LPN Example 1

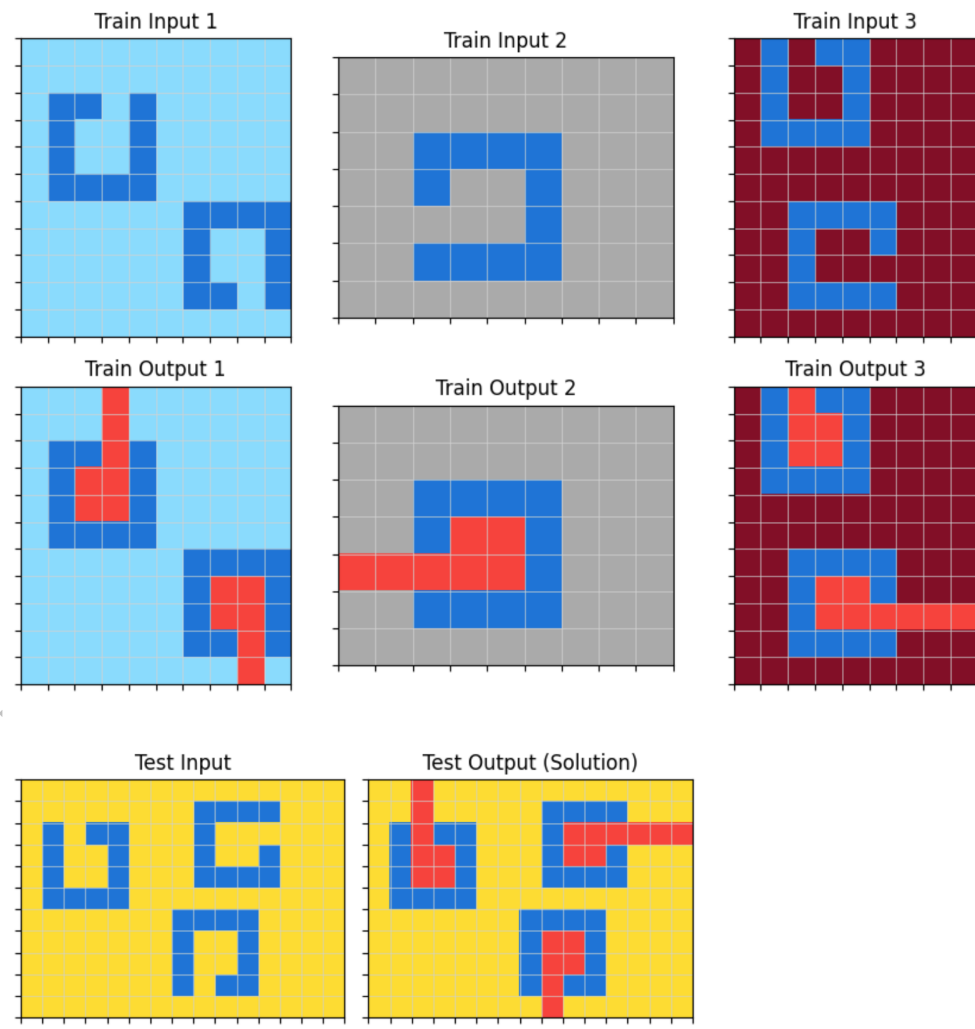


Figure 12: LPN Example 2

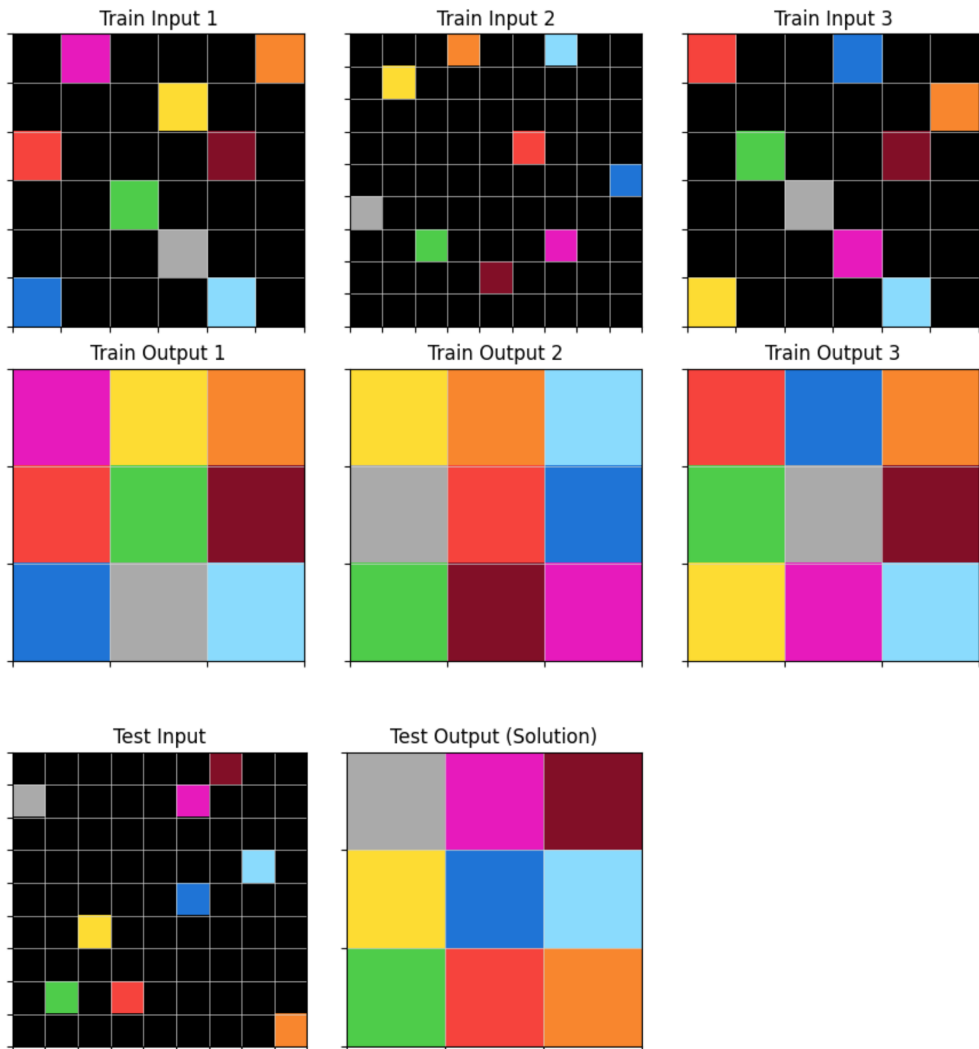


Figure 13: LPN Example 2

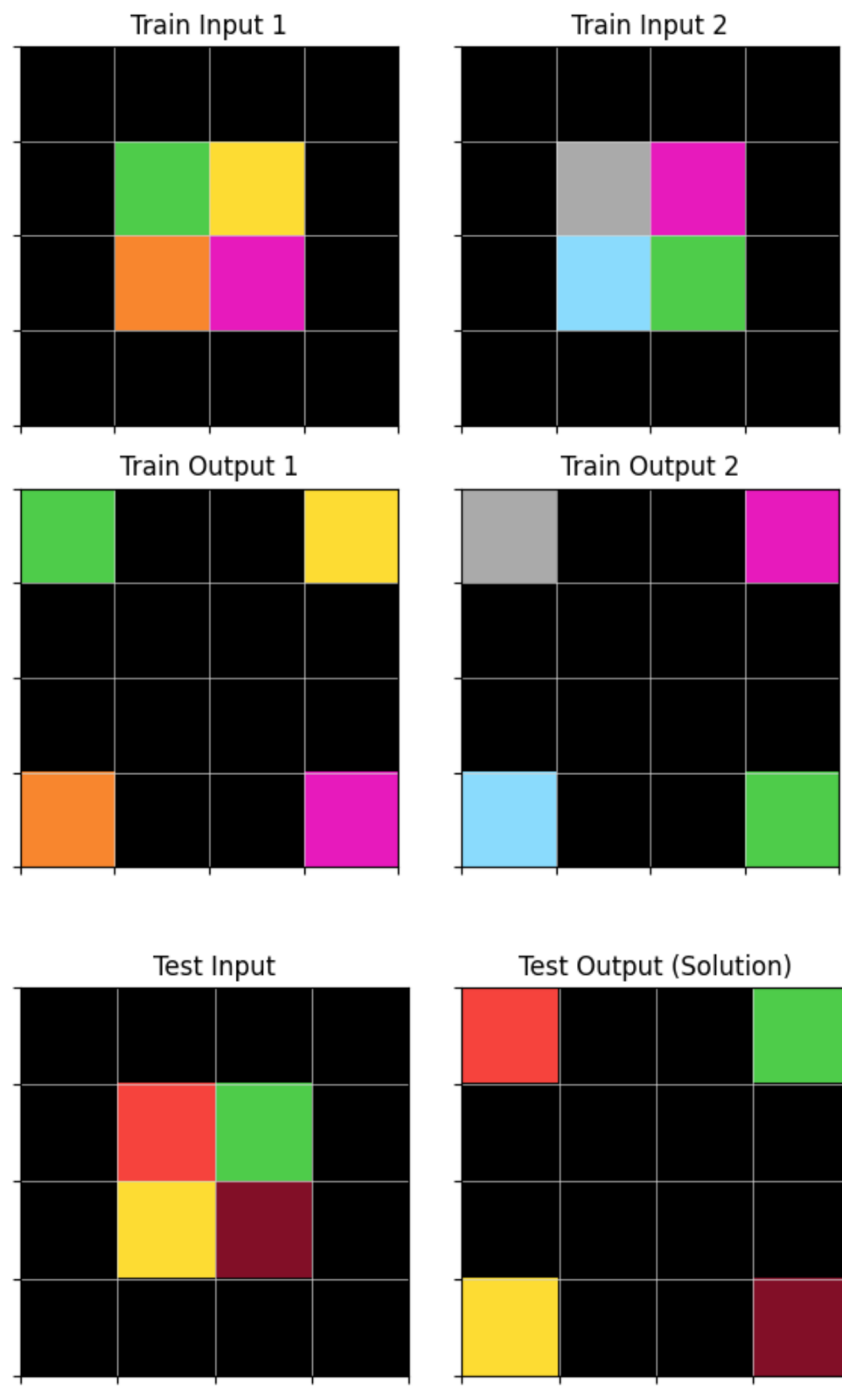


Figure 14: TTT Example 1

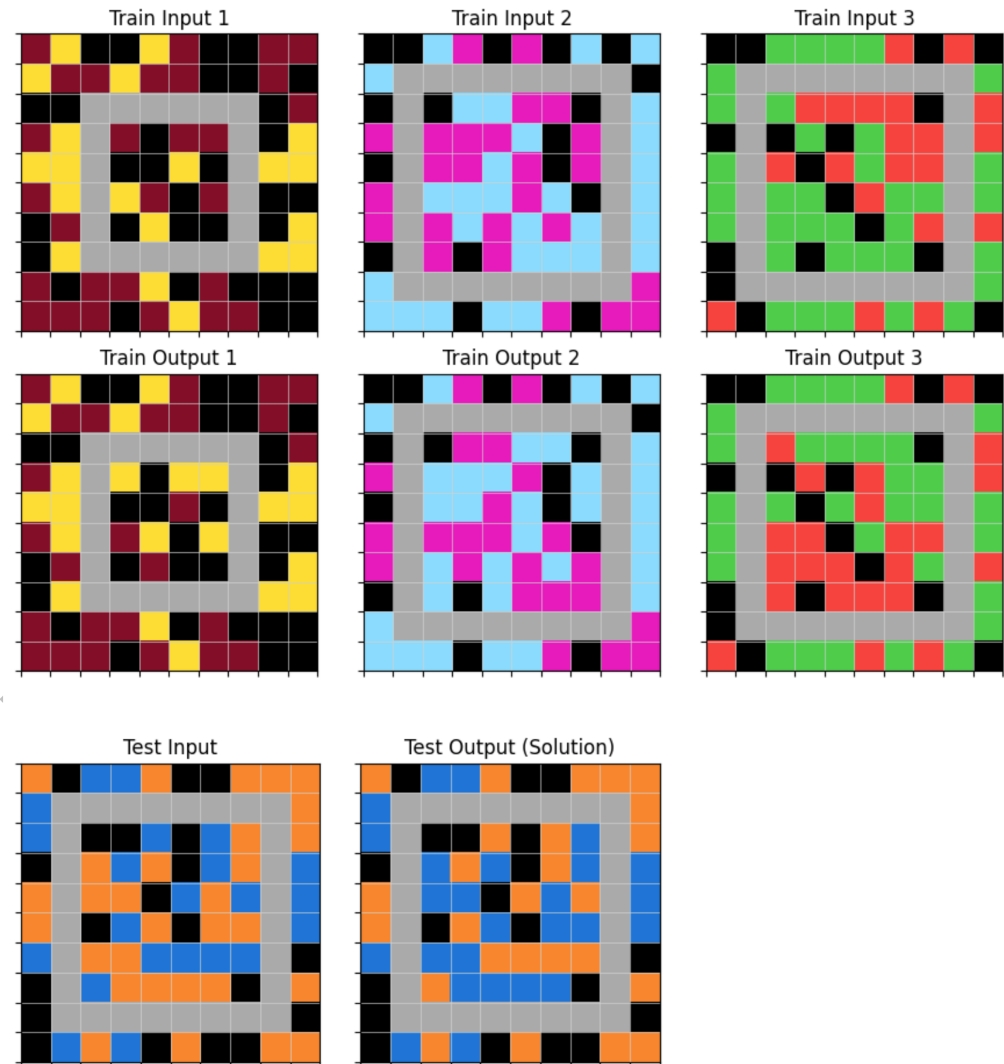


Figure 15: TTT Example 2

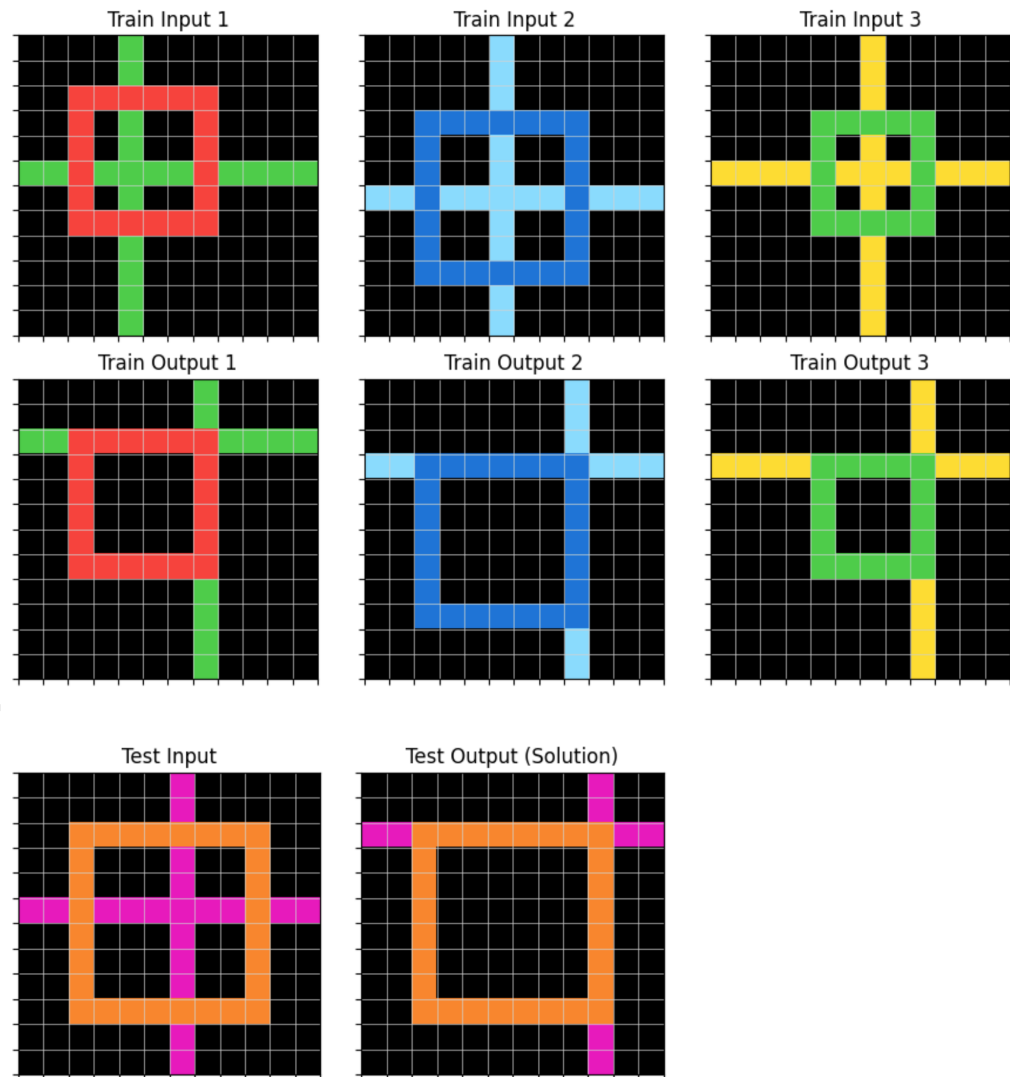


Figure 16: TTT Example 3

C LPN Algorithm

Below we outline two algorithms: first, LPN test-time inference (Algorithm 1) and its mechanism for performing inductive inference. Second, we provide the full algorithm for LPN during training (Algorithm 2).

Algorithm 1 LPN Test-Time Inference with Gradient Ascent Latent Optimization

Require: n input-output pairs (x_i, y_i) , a test input x_{n+1} , number of gradient steps K

- 1: **for** $i = 1, \dots, n$ **do** ▷ Can be done in parallel
- 2: Sample $z_i \sim q_\phi(z|x_i, y_i)$
- 3: **end for**
- 4: Initialize latent $z' \leftarrow \frac{1}{n} \sum_{i=1}^n z_i$
- 5: **for** $k = 1, \dots, K$ **do** ▷ Perform gradient ascent
- 6: $z' \leftarrow z' + \alpha \cdot \nabla_z \sum_{i=1}^n \log p_\theta(y_i|x_i, z)|_{z=z'}$
- 7: **end for**
- 8: **return** $y_{n+1} \sim p_\theta(y|x_{n+1}, z')$

Algorithm 2 LPN Training with Gradient Ascent Latent Optimization

Require: Encoder parameters ϕ , decoder parameters θ

- 1: **for** $t = 1, \dots, \text{num_training_steps}$ **do**
- 2: Sample n input-output pairs (x_i, y_i) from the same program
- 3: **for** $i = 1, \dots, n$ **do** ▷ Can be done in parallel
- 4: Sample $z_i \sim q_\phi(z|x_i, y_i)$ ▷ Using the reparameterization trick
- 5: **end for**
- 6: **for** $i = 1, \dots, n$ **do** ▷ Can be done in parallel
- 7: $z'_i \leftarrow \frac{1}{n-1} \sum_{\substack{j=1 \\ j \neq i}}^n z_j$
- 8: **for** $k = 1, \dots, K$ **do** ▷ Perform gradient ascent in the latent space
- 9: $z'_i \leftarrow z'_i + \alpha \cdot \nabla_z \sum_{j=1}^n \log p_\theta(y_j|x_j, z)|_{z=z'_i}$ ▷ Optional stop-grad on the 2nd term
- 10: **end for**
- 11: $\mathcal{L}_i \leftarrow -\log p_\theta(y_i|x_i, z'_i) + \beta \cdot D_{\text{KL}}(q_\phi(z|x_i, y_i) \parallel \mathcal{N}(0, \mathbf{I}))$
- 12: **end for**
- 13: $\mathcal{L} \leftarrow \frac{1}{n} \sum_{i=1}^n \mathcal{L}_i$ ▷ Total loss for all pairs
- 14: Update ϕ and θ via gradient descent on \mathcal{L}
- 15: **end for**

D Variational Inference

Latent Program Networks (LPNs), when operated in grad 0 mode, perform a form of variational inference. Updating the latent representation using gradients from the encoder constitutes semi-amortized variational inference [Kim et al., 2018, Marino et al., 2018].

In prior work, such as LEAPs Trivedi et al. [2021], it is assumed during training that the full representation of a program f is observable. In this setting, variational inference on programs can be conducted using a standard Variational Autoencoder (VAE) restricted to the program space. LEAPs introduce a form of variational inference via an Execution Evidence Lower Bound (ELBO), where function reconstruction is based on correctly executing the function for a given input rather than reconstructing the full program representation. The Execution ELBO is defined as:

$$\mathbb{E}_{z \sim q_\phi(z|f)} [\mathbb{E}_{x \sim p(x)} [\log p_\theta(y = f(x) | x, z)]] - \text{KL}(q_\phi(z|f) \| p(z)).$$

This formulation is advantageous because it enables learning a function that directly executes the program without requiring explicit reconstruction of the program followed by execution. In LPNs, this is critical, as the differentiable parameterization of the function executor allows backpropagation through the executor to perform program search in the latent space.

In this work, we assume that the functions generating the underlying input-output pairs are not fully observable, aligning with real-world scenarios where the data-generating functions are rarely fully known. Instead, we observe only partial data for each function, represented as a dataset $X_d = \{(x_{i,d}, y_{i,d})\}_{i=1}^{N_d}$, where each dataset d corresponds to a set of input-output pairs generated by a particular unseen function. Across D such datasets, the following objective serves as a practical approximation to the Execution ELBO:

$$\sum_{d=1}^D \sum_{i=1}^{N_d} \mathbb{E}_{z \sim q_\phi(z|X_d)} [\log p_\theta(y_{i,d} | x_{i,d}, z)] - \text{KL}(q_\phi(z|X_d) \| p(z)), \quad (7)$$

where D is the number of datasets, each representing input-output pairs from a distinct unseen function, and N_d is the number of samples in dataset d . However, this standard objective is flawed because the encoder $q_\phi(z|X_d)$ can “cheat” by encoding specific details of the pair $(x_{i,d}, y_{i,d})$ it needs to reconstruct, leading to memorization rather than capturing the general function f . To address this, we propose the Leave-One-Out (LOO) objective:

$$\sum_{d=1}^D \sum_{i=1}^{N_d} \mathbb{E}_{z \sim q_\phi(z|X_{-i,d})} [\log p_\theta(y_{i,d} | x_{i,d}, z)] - \text{KL}(q_\phi(z|X_d) \| p(z)), \quad (8)$$

where $X_{-i,d} = X_d \setminus \{(x_{i,d}, y_{i,d})\}$ denotes the dataset X_d excluding the i -th input-output pair. This objective prevents memorization by denying the encoder access to $(x_{i,d}, y_{i,d})$ when producing the latent representation z used for its reconstruction. Consequently, q_ϕ must infer the underlying function from the remaining data $X_{-i,d}$, making the LOO objective a better functional approximation of the Execution ELBO’s intent by directly promoting generalization. Training optimizes the encoder $q_\phi(z|X_d)$ and decoder $p_\theta(y | x, z)$ across multiple datasets, resulting in an amortized inference model q_ϕ that efficiently proposes an approximate posterior for any given dataset X_d .

For optimal performance on a specific test dataset X_{test} , we employ semi-amortized variational inference. First, the trained amortized encoder $q_\phi(z|X_{\text{test}})$ rapidly generates an initial latent representation z_0 . Then, with the encoder parameters ϕ and decoder parameters θ fixed, we perform instance-specific optimization starting from z_0 to find a refined latent representation z^* . This is achieved by directly maximizing the ELBO via latent z . This combination of an efficient amortized proposal and instance-specific ELBO refinement yields a superior latent program representation z^* tailored to the test problem. This procedure, known as semi-amortized variational inference, balances computational efficiency with high-quality inference.

E Hyperparameters

In this section, we outline our approach to hyperparameter search and provide full documentation of all the hyperparameters used in all reported experiments.

Hyperparameter Search To ensure a fair comparison between LPN and in-context learning, which share the same core architecture for embedding inputs and generating outputs, we kept all architectural parameters identical across methods. We conducted hyperparameter testing to determine whether to use rotational embeddings. We performed testing by repeating the decoder validation experiment with and without rotational embeddings. Rotational embeddings improved performance across all individual tasks and so was selected to be used in both the encoder and decoder of LPN.

For the ARC-AGI results, we performed a hyperparameter search over the learning rate for test time adaptation for both test-time tuning and LPN. Since these methods operate in different spaces, they are unlikely to require similar parameters, making it fairer to tune this parameter independently for each baseline. We validated on a held-out test set of unseen problems from the RE-ARC dataset. We searched over learning rates ranging from 10^{-1} to 10^{-7} . Performance was evaluated by measuring average accuracy across five FLOP measures (ranging from 2E+11 to 2E+15). For the baseline pattern task in Table 1 we choose a learning rate of 0.1 without performing hyperparameter optimisation as the experiment is simply to understand the behavior of LPN and not to optimize performance. For pattern OOD task we perform grid search for LPN and TTT over a dataset of from the strongly OOD task for 10 gradient steps, filtering out learning rates that do not decrease the test-time loss by at least 1.0%. We use these learning rates for the scaling specification size ablation also.

Validating the Decoder In section B.3, we train an LPN model on each of the `re-arc` generators corresponding to the first 5 tasks from the training set. For each task, we train the model for 10k gradient steps with a batch size of 128 and 4 pairs per specification, resulting in 5,120,000 input-output pairs. We gather all hyperparameters in table 11, common to all the tasks except 045e512c which had 4 encoder layers, 8 heads, 32 embedding dimensions per head, an MLP factor of 2.0, for a total of 8.7M parameters.

Component	Hyperparameter	Value
Encoder Transformer	Number of Layers	0
	Number of Heads	6
	Embedding Dimension per Head	16
	Latent Dimension	32
	RoPE	False
Decoder Transformer	Number of Layers	3
	Number of Heads	6
	Embedding Dimension per Head	16
	MLP Dimension Factor	1.0
	RoPE	False
Training	Number of Parameters	829k
	Training Steps	10k
	Batch Size	128
	Optimizer	AdamW
	Gradient Clipping Norm	1.0
	Learning Rate	4e-4
	Number of Rows & Columns	30, 30

Table 11: Hyperparameters for the experiments from section B.3, validating the decoder.

Pattern Task In section 5.2, we train an LPN model on a 10x10 task with 4x4 patterns. We train each method (mean, gradient ascent, etc) for a total of 20k steps with a batch size of 128 and 4 pairs per specification, resulting in a total of 10M input-output pairs.

Component	Hyperparameter	Value
Encoder Transformer	Number of Layers	2
	Number of Heads	6
	Embedding Dimension per Head	16
	MLP Dimension Factor	1.0
	Latent Dimension	32
	RoPE	False
Decoder Transformer	Number of Layers	2
	Number of Heads	6
	Embedding Dimension per Head	16
	MLP Dimension Factor	1.0
	RoPE	False
Training	Number of Parameters	973k
	Training Steps	20k
	Batch Size	128
	Prior KL Coeff	1e-4
	Optimizer	AdamW
	Gradient Clipping Norm	1.0
	Learning Rate	4e-4
	Number of Rows & Columns	10, 10
Testing	TTT Learning Rate	1e-4
	LPN Learning Rate	1e-1
	Optimizer	Adam

Table 12: Hyperparameters for the experiments from section 5.2, i.e. the pattern task.

Analyzing the Latent Space In section B.4, we train a small LPN model on a reduced version of the *Pattern* task with grids of size 4x4 and patterns of size 2x2. We used the following hyperparameters for training in table 13.

Component	Hyperparameter	Value
Encoder Transformer	Number of Layers	2
	Number of Heads	6
	Embedding Dimension per Head	12
	MLP Dimension Factor	4.0
	Latent Dimension	2
	RoPE	False
Decoder Transformer	Number of Layers	2
	Number of Heads	6
	Embedding Dimension per Head	12
	MLP Dimension Factor	4.0
	RoPE	False
Training	Number of Parameters	1M
	Training Steps	200k
	Batch Size	128
	Prior KL Coeff	1e-3
	Optimizer	AdamW
	Gradient Clipping Norm	1.0
	Learning Rate	4e-4
Testing	Number of Rows & Columns	4, 4
	TTT Learning Rate	1e-4
	LPN Learning Rate	1e-1
	Optimizer	Adam

Table 13: Hyperparameters for the experiment in section B.4, i.e. analyzing the latent space.

Out-Of-Distribution In section 5.4, we train LPN models similar to those above in the *Pattern task* and evaluate them on different distributions. We gather hyperparameters used for training in table 14.

Component	Hyperparameter	Value
Encoder Transformer	Number of Layers	4
	Number of Heads	8
	Embedding Dimension per Head	8
	MLP Dimension Factor	2.0
	Latent Dimension	32
	RoPE	False
Decoder Transformer	Number of Layers	2
	Number of Heads	8
	Embedding Dimension per Head	4
	MLP Dimension Factor	1.0
	RoPE	False
Training	Number of Parameters	1M
	Training Steps	100k
	Batch Size	128
	Prior KL Coeff	1e-4
	Optimizer	AdamW
	Gradient Clipping Norm	1.0
	Learning Rate	4e-4
Testing	Number of Rows & Columns	10, 10
	TTT Learning Rate	1e-5
	LPN Learning Rate	1e-1
	Optimizer	Adam

Table 14: Hyperparameters for the experiments from section 5.4, i.e. the study of out-of-distribution performance of LPN on the Pattern task.

ARC-AGI In table 15, we finally present the hyperparameters used for experiments on ARC-AGI (section 5.6).

Component	Hyperparameter	Value
Encoder Transformer	Number of Layers	8
	Number of Heads	8
	Embedding Dimension per Head	64
	MLP Dimension Factor	4.0
	Latent Dimension	256
	RoPE	True
	RoPE max freq	10
Decoder Transformer	Number of Layers	6
	Number of Heads	8
	Embedding Dimension per Head	64
	MLP Dimension Factor	4.0
	RoPE	True
	RoPE max freq	10
	Number of Parameters	178M
Training	Training Steps	100k
	Batch Size	256
	Prior KL Coeff	1e-4
	Optimizer	AdamW
	Gradient Clipping Norm	1.0
	Learning Rate	3e-4
	Number of Rows & Columns	30, 30
Testing	TTT Learning Rate	1e-4
	LPN Learning Rate	5e-2
	Optimizer	Adam

Table 15: Hyperparameters for the experiment in section 5.6, i.e. training LPN to solve the ARC-AGI benchmark.

F Additional Charts

F.1 Latent Program Embeddings

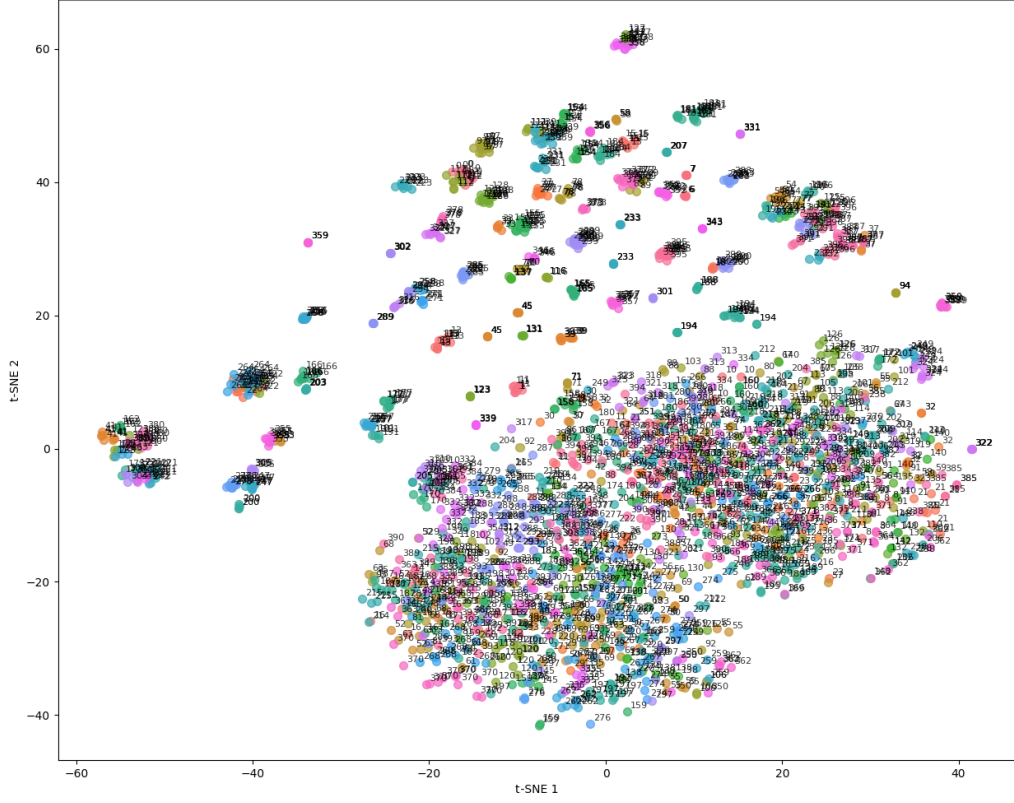


Figure 17: T-SNE visualization of the latent space of input-output pairs sampled from the `re-arc` generators. We see strong evidence that the latent embeddings encode information about programs with significant clustering in the latent space for the same programs across different input output pairs.

F.2 Decoder Gradient Field

Figure 18 visualizes the likelihood landscape of decoding the correct output conditioned on the given input for a single pattern task, while varying the latent input. The gradient contours overlaid on the plot illustrate the optimization dynamics when performing gradient-based updates in this space. The trajectories depict how gradient ascent seeks to maximize the decoding likelihood, revealing the structure of the landscape. Certain regions form basins of attraction that lead to valid solutions, while others correspond to local optima where the likelihood of decoding the correct output stagnates. This visualization highlights both the feasibility of optimizing the latent representation and the potential challenges of escaping suboptimal regions in the latent space.

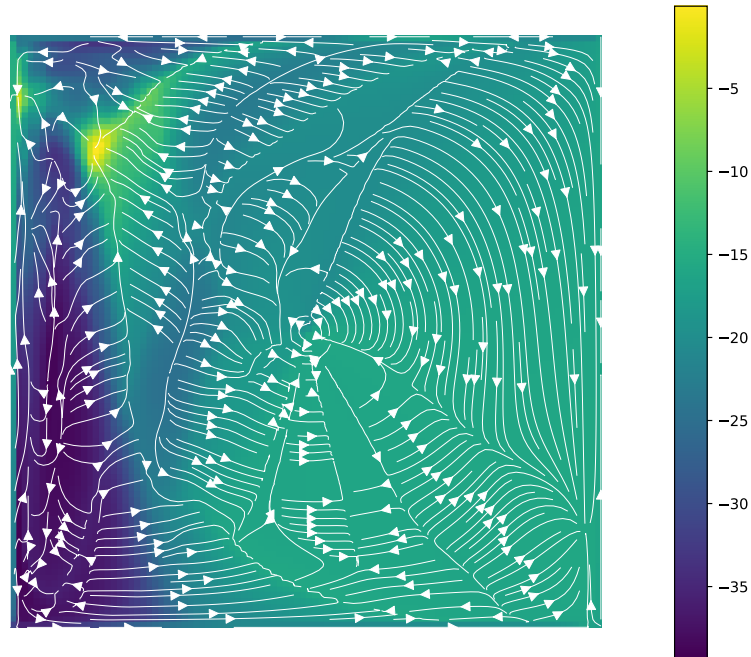


Figure 18: Visualization of the likelihood landscape for decoding the correct output conditioned on the input, as a function of the latent space.

G Architecture

In all our experiments, programs are defined in the input-output space of ARC-AGI, i.e., 2D grids whose cells can take 10 different values and have shapes (n, m) with $n, m \in [1, 30]$. We implement both the encoder and decoder as small transformers [Vaswani et al., 2017] specifically designed for this benchmark, in contrast to the more general large language models (LLMs) typically used [Wang et al., 2023].

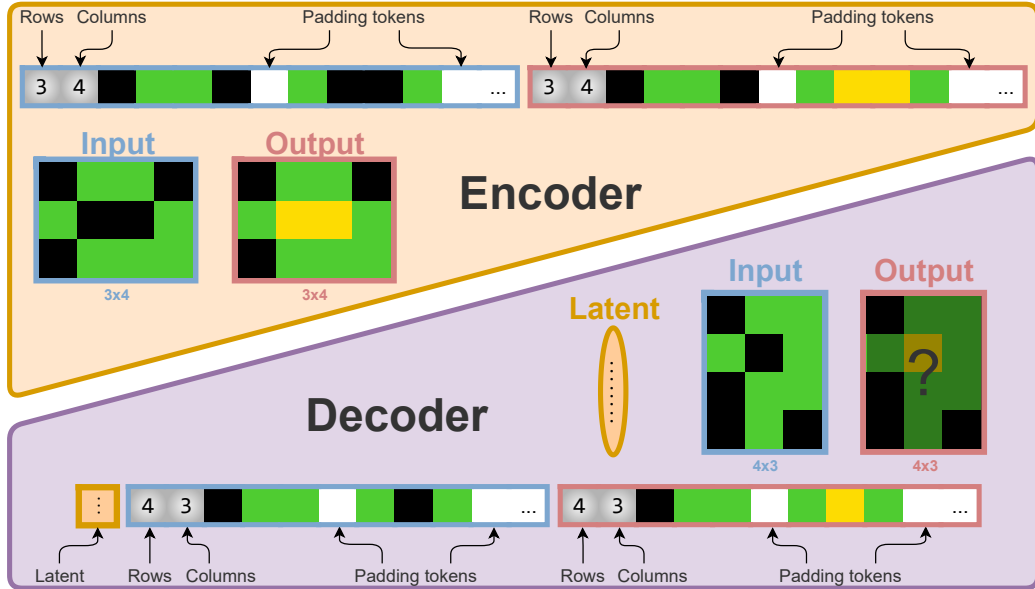


Figure 19: LPN architecture for ARC-AGI. Both the encoder and decoder are small transformers that take flattened padded grids as inputs. The actual number of rows and columns is prefixed to each sequence.

We model the input and output images as 2D grids, which we pad and flatten in a raster-scan fashion to form sequences of pixel values, each of size $30 \times 30 = 900$ (see Figure 19). Each grid sequence is prefixed with shape information, namely two extra values for the number of rows and columns, resulting in sequences of 902 values. For both the Encoder and Decoder grid positions are encoded using RoPE [Su et al., 2024]² for both row and column indices.

G.1 Encoder

The encoder processes both the input and output grids from a given pair and returns a distribution of inferred program latents underlying the task. Specifically, it outputs the mean and diagonal covariance of a multivariate normal distribution from which latents can be sampled. Each grid sequence contains 902 values, and we add an extra CLS token for the output embedding, resulting in a total sequence length of 1805 for the encoder transformer. The encoder is implemented as a standard transformer [Vaswani et al., 2017] with pre-layer normalization [Baevski and Auli, 2018, Xiong et al., 2020] and multi-head attention. To incorporate identify the input from the output we add an embedding $\text{emb}(c)$, $c \in \{0, 1\}$ is the channel index (0 for input, 1 for output). All 1800 color values (0 to 9), four shape values (1 to 30), and the CLS token are separately embedded into \mathbb{R}^H using lookup tables. Padded tokens, determined by the shape values, are masked, and the sequence is fed into multiple transformer blocks, see Appendix E for hyperparameter details. In the encoder the attention mask is non-causal, allowing all non-padded tokens to attend to each other during encoding. The CLS embedding is passed through a layer normalization and two parallel dense layers to output the mean and diagonal log-covariance of the multivariate normal distribution over latents. Sampled program latents have dimension d , which may differ from the embedding dimension H .

²<https://github.com/crowsonkb/rope-flax>

G.2 Decoder

The decoder takes an input grid and a latent program and autoregressively generates an output grid. Its design is similar to the encoder, with key differences. First, the flattened sequence is prefixed with a projection of the latent embedding. Since the decoder generates the output autoregressively, the attention mask is causal on the output grid portion of the sequence (the second half). The attention mask also dynamically accounts for padding tokens based on the predicted output shapes. The sequence embeddings corresponding to the output are extracted and projected to either shape logits for the first two embeddings or grid logits for the 900 output grid embeddings. Each output token embedding maps to logits for the next token in a raster-scan fashion. However, due to padding at each row, the last embedding of each row is mapped to the first token of the next row.

H Baselines

H.1 Transductive Baseline

We compare LPN against a transductive baseline that directly conditions on the specification without explicitly constructing a latent program representation. This approach, similar to Kolev et al. [2020], Li et al. [2024a], processes the specification by encoding and concatenating each input-output pair separately.

Encoder: The encoder maps each input-output pair to an encoding vector:

$$z_i = e_\phi(x_i, y_i) \quad \forall i \in [1, n] \quad (9)$$

where e_ϕ is a neural network parameterized by ϕ that processes individual input-output pairs.

Concatenation: Unlike LPN which searches for a single latent program, the transductive baseline uses each encoding as a token embedding in the input sequence to the transformer. Specifically, the encodings are concatenated as:

$$z_{\text{cat}} = [z_1; z_2; \dots; z_n] \quad (10)$$

where $[;]$ denotes sequence concatenation and each z_i serves as a token embedding in the transformer’s input sequence.

Decoder: The transformer decoder processes this sequence of embeddings along with the new input to generate the output:

$$\hat{y}_{n+1} \sim p_\theta(y|x_{n+1}, z_{\text{cat}}) \quad (11)$$

where the decoder attends to both the new input x_{n+1} and the sequence of specification embeddings z_{cat} .

By concatenating per-pair embeddings, we ensure a joint representation of all input-output pairs, allowing the decoder to access information from all grids during inference. Processing input-output pairs independently in the encoder serves as a strong prior for capturing high-level program features, reducing the risk of learning spurious correlations between pixels of different pairs. In contrast, methods that process all raw pairs jointly increase the encoder’s computational demands. Additionally, feeding all raw pairs directly to the decoder would complicate positional encodings, requiring simultaneous modeling of both within-pair and across-pair positions. Our approach mitigates this by encoding positional information separately within each pair at the encoder stage. The decoder then receives each pair’s embedding in a distinct position within the concatenated sequence, enabling clear differentiation between examples.

H.2 Test-Time Fine-Tuning

We implement the following test-time parameter tuning approach where the transductive model’s parameters are fine-tuned on the specification itself. Given a specification of n input-output pairs, we perform gradient updates on the model parameters to better predict each output given its input and the remaining pairs.

Update Process: Starting from the pre-trained parameters θ and ϕ (decoder and encoder respectively), for each pair (x_i, y_i) in the specification, we compute the loss:

$$\mathcal{L}_{\text{TTT}}^i(\phi, \theta) = -\log p_\theta(y_i|x_i, z_{\text{cat}}^{-i}) \quad (12)$$

where $z_{\text{cat}}^{-i} = [e_\phi(x_1, y_1); \dots; e_\phi(x_{i-1}, y_{i-1}); e_\phi(x_{i+1}, y_{i+1}); \dots; e_\phi(x_n, y_n)]$ represents the concatenated embeddings of all pairs except the i -th.

We then update the parameters using gradient descent:

$$\phi' = \phi - \alpha \nabla_\phi \sum_{i=1}^n \mathcal{L}_{\text{TTT}}^i(\phi, \theta) \quad (13)$$

$$\theta' = \theta - \alpha \nabla_\theta \sum_{i=1}^n \mathcal{L}_{\text{TTT}}^i(\phi, \theta) \quad (14)$$

where α is the learning rate for test-time adaptation.

Inference: After K steps of parameter updates, we use the tuned parameters ϕ' and θ' to make predictions on new inputs. The prediction process remains the same as the transductive baseline but uses the adapted parameters:

$$\hat{y}_{n+1} \sim p_{\theta'}(y|x_{n+1}, [e_{\phi'}(x_1, y_1); \dots; e_{\phi'}(x_n, y_n)]) \quad (15)$$